Attractive Features of Higgsino Dark Matter in the Next-to-Minimal Supersymmetric Standard Model

Yuanfang Yue[1], Junjie Cao[1,2], Fei Li[1], Zehan Li[1]

1. School of Physics, Henan Normal University, China; 2. School of Physics, Zhengzhou University, Zhengzhou, China

In the Higgsino dark matter (DM) scenario of the Minimal Supersymmetric Model (MSSM), the mixing of Gaugino and Higgsino influences the mass splitting between neutralinos predominantly composed of Higgsino and introduces coupling between the DM and Higgs bosons. These effects modify the DM-nucleon scattering cross-section, causing conflicts with the latest direct detection results from LZ experiments for both substantial and minute mixings. Consequently, the experimental measurement of DM relic density necessitates the Higgsino DM mass to be approximately 1.1 TeV. We discovered that in the Higgsino DM scenario of the Next-to-Minimal Supersymmetric Model (NMSSM), the mixing of Higgsino and Singlino introduces analogous effects, with a crucial distinction being that the current LZ experiment permits significant mixing between Singlino and Higgsino. This pronounced mixing effect effectively attenuates the interactions between Higgsino-dominated neutralinos and standard model particles, enabling DM masses exceeding roughly 660 GeV to achieve the correct relic abundance. Through analytical formulas and numerical results, we elucidated these characteristics. Our research reveals that in the NMSSM, when comprehensively examining the mixing effects of Higgsino, Gaugino, and Singlino, the properties of Higgsino DM become markedly more intricate compared to the MSSM predictions.

Corresponding author: Junjie Cao, junjiec@alumni.itp.ac.cn

1. Introduction

The existence of dark matter (DM) has been firmly established by various astronomical and cosmological observations[1], yet its particle nature remains one of the most profound mysteries in modern physics.

Among various theoretical candidates, the Higgsino, which naturally emerges from supersymmetric theories, stands out as a particularly compelling DM candidate[2][3][4][5][6][7][8][9][10][11][12][13]. In the Minimal Supersymmetric Standard Model (MSSM)[14][15][16][17], the Higgsino has the following distinctive features that make it an attractive solution to the DM puzzle, drawing on both theoretical predictions and experimental constraints:

- From a theoretical perspective, the Higgsino possesses remarkable simplicity and naturalness. As an SU(2) doublet, it represents one of the most minimal extensions to the Standard Model (SM) that can accommodate viable DM candidates. This theoretical elegance is further enhanced by its crucial role in gauge coupling unification, where the Higgsino provides necessary contributions to achieve precise unification at high energies. Additionally, in the MSSM, Higgsino DM depends only on a limited number of parameters, minimizing theoretical ambiguities and providing a clean framework for both theoretical study and experimental interpretation.

- From a theoretical perspective, the Higgsino possesses remarkable simplicity and naturalness[18][19][20][21][22]. As an SU(2) doublet, it represents one of the most minimal extensions to the Standard Model (SM) that can accommodate viable DM candidates[23][24]. This theoretical elegance is further enhanced by its crucial role in gauge coupling unification, where the Higgsino provides necessary contributions to achieve precise unification at high energies[25][26][27] and is readily embedded into theories like split SUSY[28][29][30][31]. Additionally, in the MSSM, Higgsino DM depends only on a limited number of parameters, minimizing theoretical ambiguities and providing a clean framework for both theoretical study and experimental interpretation[10][32].

- A particularly intriguing aspect of Higgsino DM is its mass scale. To produce the observed DM relic density, the Higgsino mass needs to be around 1.1 TeV[33][34][28][11][35][36]. This mass scale, determined by the interplay between electroweak interactions and freeze-out dynamics, carries profound physical significance. Specifically, it is not only preferred by natural electroweak symmetry breaking, as indicated by the expression of the Z boson mass[37], but also explains the current null results from the Large Hadron Collider (LHC) searches for supersymmetry[38]. The latter aspect is characterized by the fact that the LHC's sensitivity to both electroweakly and strongly produced supersymmetric particles decreases monotonously as the DM becomes heavy, making it challenging to detect their signals when the DM mass is larger than approximately $1 TeV$[38]. This alignment between theoretical

prediction and experimental observation may be viewed as a compelling hint for the Higgsino DM scenario.

The phenomenology of Higgsino DM exhibits rich features in terms of experimental detection[39][40][41][42]. In direct detection experiments, the interaction of Higgsino DM with nuclei depends on its mixing with heavier Gaugino states (e.g., Wino or Bino). When Gaugino component mixing increases, the scattering cross-section becomes large[43][44][45][46], rendering such models stringently constrained by leading DM direct detection experiments such as PandaX-4T[47], XENONnT[48], and LUX-ZEPLIN (LZ)[49][50]. Current observations suggest that Gaugino masses must be larger than around 2 TeV to avoid over-enhancing the Higgsino's spin-independent (SI) scattering cross-section[44][51][32][52]. Furthermore, when the Gauginos are heavier than $10^8\,\mathrm{GeV}$, the mass difference between the lightest neutral Higgsino components is smaller than 100 KeV[42]. In this case, inelastic DM-nucleon scattering processes in direct detection are kinematically allowed with an unsuppressed spin-dependent (SD) cross-section, which has been very tightly constrained by current detection experiments. These features yield a unique phenomenological window for the Higgsino, where the Gauginos with masses between 2 TeV and $10^8\,\mathrm{GeV}$ naturally evade current experimental bounds.

In addition, unlike Wino DM which acts as another popular candidate, Higgsino DM can avoid indirect detection constraints by lacking significant Sommerfeld enhancement in its annihilation cross-section due to the larger mass splitting between the charged and neutral components of the Higgsino field[53][54][55]. This makes it challenging for current gamma-ray[56][57] or neutrino telescopes[58] to detect Higgsino annihilation signals, adding to the difficulty in probing this candidate with indirect detection experiments[53].

- Higgsino DM exhibits unique collider signatures due to the small mass splittings among its charged and neutral components. The charged Higgsino (chargino) can manifest as either missing transverse energy (MET) or disappearing tracks in high-energy collisions[59]. These signals are a robust prediction of electroweak-scale Higgsino DM and present both challenges and opportunities for future experiments[60][61][62][11]. Advanced detection techniques, such as optimized triggers for soft visible decay products and improved track reconstruction algorithms, are currently being developed, making this an active area of theoretical and experimental research[63][32]

In conclusion, Higgsino DM is regarded as one of the most theoretically elegant and experimentally compelling candidates for addressing the DM enigma. Its profound connection to supersymmetry, compatibility with current experimental constraints, and distinctive phenomenological characteristics have established it as a central focus of ongoing research.

While the MSSM offers a robust theoretical framework for studying Higgsino DM, it faces the challenging μ-parameter problem. Although this issue can be addressed through the well-known Giudice-Masiero mechanism[64], implementing this solution introduces significant fine-tuning in electroweak symmetry breaking when considering the LHC's supersymmetry search results and the DM experimental detection results[65][66][67][68].

To address these challenges, we extend our investigation of Higgsino DM to the Next-to-Minimal Supersymmetric Standard Model (NMSSM), which serves as a natural and minimal extension of the MSSM[69][70][71]. This model incorporates an additional gauge singlet Higgs superfield, $\hat{S}$, that can dynamically generate an effective μ parameter when its scalar component develops a vacuum expectation value (vev). This mechanism substantially improves the stability of the electroweak vacuum, making the theoretical framework more appealing[36][72][73].

In the NMSSM, the fermionic component of $\hat{S}$, known as the Singlino, can substantially mix with the Higgsino field, thereby altering key properties of Higgsino DM, such as its mass splitting from other Higgsino-like particles and its interactions with nuclei[74][36]. Consequently, Higgsino DM exhibits novel features in DM annihilation and DM–nucleon scattering processes.

Given that these characteristics have been scarcely discussed in previous literatures, this study aims to comprehensively examine them. Notably, in the Z_3-invariant NMSSM, achieving substantial Higgsino-Singlino mixing necessitates near–degeneracy of the fields' masses, constraining the Yukawa couplings λ and κ to satisfy $\lambda \simeq 2\kappa$[70]. As will be illustrated below, this constraint limits the properties of Higgsino DM. Therefore, we conduct our investigation within the framework of the General NMSSM (GNMSSM)[75][76][77] to provide a more complete characterization of these properties. We will show that the properties of the Higgsino DM in the NMSSM are more flexible than those in the MSSM, while remaining consistent with various experimental constraints.

The remainder of this paper is structured as follows. Section 2 delineates the distinctive characteristics of the GNMSSM, with a particular focus on the analytical examination of the Higgsino DM properties through expressions of various observables. Section 3 elucidates the research methodology and

numerical outcomes that highlight the novel aspects of the Higgsino DM. Finally, Section 5 offers a comprehensive summary of the key research findings.

2. Theoretical preliminaries

2.1. Basics of the GNMSSM

The GNMSSM extends the MSSM by introducing a gauge singlet superfield $\hat{S}$, which does not carry any baryonic or leptonic number. Consequently, its Higgs sector comprises $\hat{S}$ alongside two $SU(2)_L$ doublet superfields, $\hat{H}_u = (\hat{H}_u^+, \hat{H}_u^0)$ and $\hat{H}_d = (\hat{H}_d^0, \hat{H}_d^-)$. The general form of the GNMSSM superpotential is given by[70]:

$$W_{\text{GNMSSM}} = W_{\text{Yukawa}} + \lambda \hat{S} \hat{H}_u \cdot \hat{H}_d + \frac{\kappa}{3} \hat{S}^3 + \mu \hat{H}_u \cdot \hat{H}_d + \frac{1}{2} \mu' \hat{S}^2 + \xi \hat{S}, \qquad (2.1)$$

where W_{Yukawa} contains the quark and lepton Yukawa interactions from the MSSM superpotential but excludes the μ-term, and the dimensionless couplings λ and κ parameterize the Higgs-sector interactions, similar to the Z_3-NMSSM. The parameters μ, μ', and ξ describe Z_3-symmetry-violating effects, which help address the tadpole problem[78][70] and the cosmological domain-wall problem in the Z_3-NMSSM[79][80][81]. Since one of these parameters can be eliminated by shifting $\hat{S}$ with a constant and redefining the other parameters[82], we set $\xi = 0$ without loss of generality. Previous studies indicate that μ and μ' can naturally lie in the range of a few hundred GeV from the breaking of the fundamental discrete R-symmetry $\mathbb{Z}_4^R$ or $\mathbb{Z}_8^R$ at high energies[79][83][84][82][85]. These parameters can substantially modify the properties of neutral Higgs bosons and neutralinos, leading to a richer phenomenology than those in the Z_3-NMSSM and MSSM, which forms the main focus of this study.

In contrast to the MSSM, the GNMSSM contains both the traditional μ-term $\mu \hat{H}_u \cdot \hat{H}_d$ and a dynamically generated μ-term $\lambda \hat{S} \hat{H}_u \cdot \hat{H}_d$. When the scalar component of $\hat{S}$ develops a vev $\langle S \rangle \equiv v_s / \sqrt{2}$, the effective μ parameter is given by $\mu_{tot} = \lambda v_s / \sqrt{2} + \mu$. This dynamical generation provides additional flexibility in addressing the naturalness problems associated with the μ-term in the MSSM. In particular, if $\lambda v_s / \sqrt{2} \gg \mu$, μ_{tot} is predominantly generated dynamically.

2.2. The Higgs Sector

In the GNMSSM, the soft SUSY-breaking terms in the Higgs sector include trilinear interactions involving the singlet and doublet fields, as well as conventional mass terms. These terms are expressed as:

$$-\mathcal{L}_{\mathrm{soft}} = \left[\lambda A_\lambda S H_u \cdot H_d + \frac{1}{3}\kappa A_\kappa S^3 + m_3^2 H_u \cdot H_d + \frac{1}{2}S^2 + \xi' S + \mathrm{h.c.} \right] \tag{2.2}$$
$$+ m_{H_u}^2 |H_u|^2 + m_{H_d}^2 |H_d|^2 + m_S^2 |S|^2,$$

After electroweak symmetry breaking, the CP-even and CP-odd Higgs fields mix to form three and two mass eigenstates, respectively. In this context, it is more intuitive to work with physical parameters rather than the original Lagrangian parameters. The key physical parameters are given as the follows[77]:

- m_A: This parameter represents the mass scale of the heavy MSSM-like CP-odd Higgs boson. It is defined as

$$m_A^2 = \left[\lambda v_s(\sqrt{2}A_\lambda + \kappa v_s + \sqrt{2}\mu') + 2m_3^2 \right] / \sin 2\beta. \tag{2.3}$$

- m_B: This parameter characterizes the mass scale of the CP-even singlet Higgs. It is related to the original parameters by

- m_B: This parameter characterizes the mass scale of the CP-even singlet Higgs. It is related to the original parameters by

$$m_B^2 = \frac{(A_\lambda + \mu')\sin 2\beta}{2\sqrt{2}v_s}\lambda v^2 + \frac{\kappa v_s}{\sqrt{2}}\left(A_\kappa + 2\sqrt{2}\kappa v_s + 3\mu'\right) - \frac{\mu}{\sqrt{2}v_s}\lambda v^2 - \frac{\sqrt{2}}{v_s}\xi'. \tag{2.4}$$

- m_C: This parameter describes the mass scale of the CP-odd singlet Higgs, determined by

$$m_C^2 = \frac{(A_\lambda + 2\sqrt{2}\kappa v_s + \mu')\sin 2\beta}{2\sqrt{2}v_s}\lambda v^2 - \frac{\kappa v_s}{\sqrt{2}}\left(3A_\kappa + \mu'\right) - \frac{\mu}{\sqrt{2}v_s}\lambda v^2 - 2m_{S'}^2 - \frac{\sqrt{2}}{v_s}\xi'. \tag{2.5}$$

- m_N and μ_{tot}: These denote the Singlino and the Higgsino masses, respectively, and are given by

$$m_N = \mu' + \sqrt{2}\kappa v_s, \quad \mu_{tot} = \mu + \lambda v_s/\sqrt{2}. \tag{2.6}$$

In the basis defined by $(H_{NSM} \equiv \cos\beta \mathrm{Re}(H_u^0) - \sin\beta \mathrm{Re}(H_d^0),\ H_{SM} \equiv \sin\beta \mathrm{Re}(H_u^0) + \cos\beta \mathrm{Re}(H_d^0),$ $\mathrm{Re}[S])$, elements of the CP-even mass matrix read as[77]

$$\mathcal{M}_{S,11}^2 = m_A^2 + \frac{1}{2}(2m_Z^2 - \lambda^2 v^2)\sin^2 2\beta, \quad \mathcal{M}_{S,12}^2 = -\frac{1}{4}(2m_Z^2 - \lambda^2 v^2)\sin 4\beta,$$
$$\mathcal{M}_{S,13}^2 = -\frac{\lambda v}{\sqrt{2}}(A_\lambda + m_N)\cos 2\beta, \quad \mathcal{M}_{S,22}^2 = m_Z^2 \cos^2 2\beta + \frac{1}{2}\lambda^2 v^2 \sin^2 2\beta, \tag{2.7}$$
$$\mathcal{M}_{S,23}^2 = \frac{\lambda v}{\sqrt{2}}\left[2\mu_{tot} - (A_\lambda + m_N)\sin 2\beta\right], \quad \mathcal{M}_{S,33}^2 = m_B^2.$$

Similarly, in the basis $(A_{NSM} \equiv \cos\beta \mathrm{Im}(H_u^0) - \sin\beta \mathrm{Im}(H_d^0),\ \mathrm{Im}[S])$, the CP-odd mass matrix elements are[77]

$$\mathcal{M}_{P,11}^2 = m_A^2, \quad \mathcal{M}_{P,22}^2 = m_C^2, \quad \mathcal{M}_{P,12}^2 = \frac{\lambda v}{\sqrt{2}}(A_\lambda - m_N). \tag{2.8}$$

Here, $\tan\beta$ is the ratio of the Higgs doublet vevs, i.e., $\tan\beta \equiv v_u/v_d$, with $v = \sqrt{v_u^2 + v_d^2} \simeq 246\,\mathrm{GeV}$.

Diagonalizing these matrices yields the mass eigenstates $h_i = \{h, H, h_s\}$ and $a_j = \{A_H, A_s\}$, which are related to the interaction states via

$$h_i = V_{h_i}^{\mathrm{NSM}} H_{\mathrm{NSM}} + V_{h_i}^{\mathrm{SM}} H_{\mathrm{SM}} + V_{h_i}^{\mathrm{S}} \mathrm{Re}[S], \tag{2.9}$$

$$a_j = V_{P,a_j}^{\mathrm{NSM}} A_{\mathrm{NSM}} + V_{P,a_j}^{\mathrm{S}} \mathrm{Im}[S]. \tag{2.10}$$

In this notation, h corresponds to the scalar discovered at the LHC, H and A_H represent heavy doublet-dominated Higgs bosons and h_s and A_s are singlet-dominated states. For convenience, these states are also labeled as h_i (i=1,2,3) and A_j (j=1,2) in ascending mass orders, i.e., $m_{h_1} < m_{h_2} < m_{h_3}$ and $m_{A_1} < m_{A_2}$ in this study. The model also predicts a pair of charged Higgs bosons, $H^+ = \cos\beta H_u^+ + \sin\beta H_d^+$, with masses given by[70]

$$m_{H^\pm}^2 = m_A^2 + m_W^2 - \frac{1}{2}\lambda^2 v^2. \tag{2.11}$$

Several important features characterize the GNMSSM Higgs sector:

- **Higgs mass spectrum**

  The LHC data reveal that one eigenstate must exhibit SM-like couplings and have a mass of approximately 125 GeV[86][87]. Additionally, the doublet-like states should be heavier than approximately 1 TeV, while singlet-dominated states are less tightly restricted[88].

- **Doublet-Singlet mixing**

  The mixing of the singlet states with doublet fields is proportional to λ. In the decoupling limit $\lambda \to 0$, the singlet fields effectively separate from the Higgs doublets, and the masses m_B, m_C, and m_N can be treated as physical particle masses with high accuracy.

- **Heavy charged Higgs approximation**

  When the charged Higgs bosons are heavy, they are approximately degenerate in mass with the CP-even scalar H and the CP-odd scalar A_H. Simplified expressions for the singlet-dominated states and their mixing parameters can be used in this limit[89]:

$$m_{h_s}^2 \simeq m_B^2 - \frac{\mathcal{M}_{S,13}^4}{m_A^2 - m_B^2}, \quad m_{A_s}^2 \simeq m_C^2 - \frac{\mathcal{M}_{P,12}^4}{m_A^2 - m_C^2}, \quad \frac{V_{P,A_s}^{\mathrm{NSM}}}{V_{P,A_s}^{\mathrm{S}}} = \frac{\mathcal{M}_{P,12}^2}{m_{A_s}^2 - m_A^2} \simeq 0,$$

$$\frac{V_h^{\mathrm{S}}}{V_h^{\mathrm{SM}}} \simeq \frac{\mathcal{M}_{S,23}^2}{m_h^2 - m_B^2}, \quad V_h^{\mathrm{NSM}} \sim 0, \quad V_h^{\mathrm{SM}} \simeq \sqrt{1 - \left(\frac{V_h^{\mathrm{S}}}{V_h^{\mathrm{SM}}}\right)^2} \sim 1, \tag{2.12}$$

$$\frac{V_{h_s}^{\mathrm{SM}}}{V_{h_s}^{\mathrm{S}}} \simeq \frac{\mathcal{M}_{S,23}^2}{m_{h_s}^2 - m_h^2}, \quad V_{h_s}^{\mathrm{NSM}} \sim 0, \quad V_{h_s}^{\mathrm{S}} \simeq \sqrt{1 - \left(\frac{V_{h_s}^{\mathrm{SM}}}{V_{h_s}^{\mathrm{S}}}\right)^2} \sim 1.$$

These formulae indicate that $V_h^{\mathrm{S}} \simeq -V_{h_s}^{\mathrm{SM}}$ and they are all proportional to λ.

- **Parameter determination**

  Using the physical masses m_A, m_B, m_C, m_N, and μ_{tot} as inputs, the original Lagrangian parameters

can be determined[77]:

$$\mu = \mu_{tot} - \frac{\lambda}{\sqrt{2}} v_s, \quad \mu' = m_N - \sqrt{2}\kappa v_s$$

$$m_3^2 = \frac{m_A^2 \sin 2\beta}{2} - \lambda v_s \left(\frac{\kappa v_s}{2} + \frac{\mu'}{\sqrt{2}} + \frac{A_\lambda}{\sqrt{2}} \right)$$

$$\xi' = \frac{v_s}{\sqrt{2}} \left[\frac{(A_\lambda + \mu') \sin 2\beta}{2\sqrt{2} v_s} \lambda v^2 + \frac{\kappa v_s}{\sqrt{2}} (A_\kappa + 2\sqrt{2}\kappa v_s + 3\mu') - \frac{\mu}{\sqrt{2} v_s} \lambda v^2 - m_B^2 \right],$$

$$m_S'^2 = \frac{1}{2} \left[m_B^2 - m_C^2 + \lambda\kappa \sin 2\beta v^2 - 2\sqrt{2}\kappa v_s \left(A_\kappa + \frac{\kappa}{\sqrt{2}} v_s + \mu' \right) \right]. \tag{2.13}$$

- **Parameter dependence**

In the Higgs sector, eight out of eleven parameters, namely $\tan\beta$, λ, A_λ, m_A, m_B, m_C, m_N, and μ_{tot}, uniquely determine the Higgs mass matrices. The remaining three parameters, κ, A_κ, and v_s, play a distinct role in governing the triple Higgs coupling strengths[77]. In the vanishing tadpole scenario delineated by $\xi' = 0$, A_κ takes the form[77]:

$$\kappa A_\kappa = \frac{\sqrt{2} m_B^2}{v_s} + \frac{\lambda\mu v^2}{v_s^2} - \frac{\lambda(A_\lambda + m_N - \sqrt{2}\kappa v_s)v^2 \sin 2\beta}{2 v_s^2} + \sqrt{2}\kappa^2 v_s - 3\kappa m_N. \tag{2.14}$$

Moreover, investigations of the light h_s scenario usually employ a parameterization of $\mathcal{M}_{S,23}^2$ as $\mathcal{M}_{S,23}^2 = \sqrt{2}\lambda\delta v\mu_{tot}$, where δ is defined by $\delta \equiv [2\mu_{tot} - (A_\lambda + m_N)\sin 2\beta]/(2\mu_{tot})$[90]. This parameter δ serves as a measure of the cancellation between different terms in $\mathcal{M}_{S,23}^2$. A key advantage of this parameterization emerges when δ takes small values: it naturally accommodates larger values of λ while maintaining consistency with the LHC measurements of the 125 GeV Higgs properties.

2.3. Neutralino Sector

The mixing between the fermionic partners for the neutral Higgs bosons and the gauginos gives rise to five neutralinos and two charginos, denoted by $\tilde{\chi}_i^0$ ($i = 1, \ldots, 5$) and $\tilde{\chi}_i^\pm$ ($i = 1, 2$), respectively. In the gauge eigenstate basis $\psi^0 = (-i\tilde{B}, -i\tilde{W}, \tilde{H}_d^0, \tilde{H}_u^0, \tilde{S})$, we can express the symmetric neutralino mass matrix as[70]:

$$M_{\tilde{\chi}^0} = \begin{pmatrix} M_1 & 0 & -m_Z \sin\theta_W \cos\beta & m_Z \sin\theta_W \sin\beta & 0 \\ & M_2 & m_Z \cos\theta_W \cos\beta & -m_Z \cos\theta_W \sin\beta & 0 \\ & & 0 & -\mu_{tot} & -\frac{1}{\sqrt{2}}\lambda v \sin\beta \\ & & & 0 & -\frac{1}{\sqrt{2}}\lambda v \cos\beta \\ & & & & m_N \end{pmatrix}, \tag{2.15}$$

where M_1 and M_2 represent gaugino soft-breaking masses, and we define $s_W \equiv \sin\theta_W$, and $c_w \equiv \cos\theta_W$. The physical mass eigenstates $\tilde{\chi}_i^0$ are obtained through diagonalization using a rotation matrix N:

$$\tilde{\chi}_i^0 = N_{i1}\psi_1^0 + N_{i2}\psi_2^0 + N_{i3}\psi_3^0 + N_{i4}\psi_4^0 + N_{i5}\psi_5^0, \tag{2.16}$$

where the index i runs from 1 to 5, with states ordered by increasing mass. The coefficients N_{i3} and N_{i4} represent the $\tilde{H}_d^0$ and $\tilde{H}_u^0$ components in $\tilde{\chi}_i^0$, respectively. We call $\tilde{\chi}_1^0$ the Higgsino-dominated DM if $(N_{13}^2 + N_{14}^2) > 0.5$.

When the gauginos become very massive, they effectively decouple from the Higgsino–Singlino system. This decoupling reduces the original 5×5 neutralino mass matrix to a simpler 3×3 matrix that captures the essential Higgsino DM properties. Working in the basis $(\tilde{H}_1 \equiv (\tilde{H}_d + \tilde{H}_u)/\sqrt{2}$, $\tilde{H}_2 \equiv (\tilde{H}_d - \tilde{H}_u)/\sqrt{2}, \tilde{S})$, this reduced matrix takes the form:

$$M_{\tilde{\chi}^0} = \begin{pmatrix} -\mu_{\text{tot}} & 0 & -\frac{1}{2}\lambda v(\sin\beta + \cos\beta) \\ 0 & \mu_{\text{tot}} & -\frac{1}{2}\lambda v(\sin\beta - \cos\beta) \\ - & - & m_N \end{pmatrix}. \tag{2.17}$$

The corresponding mass eigenstates in this reduced basis can be expressed as:

$$\tilde{\chi}_i^0 = N_{i1}'\tilde{H}_1 + N_{i2}'\tilde{H}_2 + N_{i3}'\tilde{S}, \tag{2.18}$$

where the elements of the new rotation matrix N' are given by $N_{i1}' \equiv (N_{i3} + N_{i4})/\sqrt{2}$, $N_{i2}' \equiv (N_{i3} - N_{i4})/\sqrt{2}$, and $N_{i3}' \equiv N_{i5}$.

Our subsequent analysis focuses on scenarios featuring substantial mixing between $\tilde{H}_1$ and $\tilde{S}$ states. We parameterize m_N using a positive number d, such that $m_N = -(1+d)\mu_{\text{tot}}$, and we work under the assumptions $\mu_{\text{tot}} > 0$ and $\mu_{\text{tot}} \gg d\mu_{\text{tot}} > \lambda v$. Following the methodology outlined in Ref. [91], we derive approximate expressions for neutralino masses and mixing parameters:

$$m_{\tilde{\chi}_{1,3}^0} \simeq -\mu_{\text{tot}} \pm \frac{\sqrt{(d\mu_{\text{tot}})^2 + \lambda^2 v^2(1 + \sin 2\beta)} \mp d\mu_{\text{tot}}}{2},$$
$$m_{\tilde{\chi}_2^0} \simeq \mu_{\text{tot}} + \frac{\lambda^2 v^2(1 - \sin 2\beta)}{8\mu_{\text{tot}}}, \tag{2.19}$$

which implies

$$m_{\tilde{\chi}_1^0} \simeq -\mu_{\text{tot}} + \frac{\lambda^2 v^2(1 + \sin 2\beta)}{4d\mu_{\text{tot}}}, \quad m_{\tilde{\chi}_2^0} \simeq \mu_{\text{tot}}, \quad m_{\tilde{\chi}_3^0} \simeq -\mu_{\text{tot}} - d\mu_{\text{tot}}, \tag{2.20}$$

if $d\mu_{\text{tot}}$ is significantly larger than λv, and

$$\frac{N'_{i1}}{N'_{i3}} = -\frac{\lambda v(\sin\beta + \cos\beta)}{2(\mu_{\text{tot}} + m_{\tilde{\chi}_i^0})}, \quad \frac{N'_{i2}}{N'_{i3}} = \frac{\lambda v(\sin\beta - \cos\beta)}{2(\mu_{\text{tot}} - m_{\tilde{\chi}_i^0})}. \tag{2.21}$$

The Singlino component in $\tilde{\chi}_i^0$ can be expressed as

$$
\begin{aligned}
(N'_{i3})^2 &= \left(1 + \left(\frac{N'_{i1}}{N'_{i3}}\right)^2 + \left(\frac{N'_{i2}}{N'_{i3}}\right)^2\right)^{-1} \\
&= \frac{2(m_{\tilde{\chi}_i^0}^2 - \mu_{\text{tot}}^2)^2}{2(m_{\tilde{\chi}_i^0}^2 - \mu_{\text{tot}}^2)^2 + \lambda^2 v^2(m_{\tilde{\chi}_i^0}^2 + \mu_{\text{tot}}^2 - 2\sin 2\beta \mu_{\text{tot}} m_{\tilde{\chi}_i^0})}.
\end{aligned}
\tag{2.22}
$$

For the parameter space relevant to our study, which is characterized by $\lambda \sim \mathcal{O}(0.1)$ and $\mu_{\text{tot}} > 600\,\text{GeV}$, the rotation matrix N' can be approximated by a simpler form:

$$N' \simeq \begin{pmatrix} \cos\theta & 0 & \sin\theta \\ 0 & 1 & 0 \\ -\sin\theta & 0 & \cos\theta \end{pmatrix}, \tag{2.23}$$

where the Higgsino-Singlino mixing angle is given by

$$
\begin{aligned}
\tan\theta &= \frac{d\mu_{\text{tot}} - \sqrt{(d\mu_{\text{tot}})^2 + \lambda^2 v^2(1 + \sin 2\beta)}}{\lambda v(\sin\beta + \cos\beta)} \\
&\simeq -\frac{\lambda v}{2d\mu_{\text{tot}}}(\sin\beta + \cos\beta), \quad \text{if } d\mu_{\text{tot}} \gg \lambda v.
\end{aligned}
\tag{2.24}
$$

This simplified representation of N' significantly facilitates the analysis presented in subsequent sections.

2.4. DM Relic Density

The relic density of Weakly Interacting Massive Particle (WIMP) DM can be calculated from its thermally averaged annihilation cross-section in the non-relativistic limit. In the absence of co-annihilation, this cross-section is given by[2]:

$$\langle \sigma_A v \rangle = a + b\langle v^2 \rangle + \mathcal{O}(\langle v^4 \rangle) \approx a + \frac{6b}{x}, \tag{2.25}$$

where a represents the velocity-independent s-wave contribution, and b incorporates both s- and p-wave components. The dimensionless parameter $x \equiv m_{\tilde{\chi}_1^0}/T$ characterizes the ratio of DM mass to the thermal bath temperature T in the early Universe. Furthermore, by solving the Boltzmann equation from the freeze-out temperature to the present day, one obtains the current relic density[89]:

$$\Omega h^2 = 0.12 \left(\frac{80}{g_*}\right)^{1/2} \left(\frac{x_F}{25}\right) \left(\frac{2.3 \times 10^{-26}\,\text{cm}^3/\text{s}}{\langle \sigma v \rangle_{x_F}}\right), \tag{2.26}$$

where $g_* \sim 80$ denotes the effective number of relativistic degrees of freedom at freeze-out, and $x_F \equiv m/T_F \sim 25$ is determined by the freeze-out condition[89]. In scenarios with co-annihilation, the relic density is computed in a similar way, as shown by Eq. 15 in Ref.[92].

For the Higgsino DM in this study, the observed relic density is primarily achieved through two types of processes: direct annihilation $\tilde{\chi}_1^0 \tilde{\chi}_1^0 \rightarrow XY$ (where X and Y are SM particles) and co-annihilation processes involving channels such as $\tilde{\chi}_{1,2,3}^0 \tilde{\chi}_1^\pm$, $\tilde{\chi}_1^0 \tilde{\chi}_2^0$, $\tilde{\chi}_1^\pm \tilde{\chi}_1^\mp \rightarrow XY$. The effective annihilation cross-section is given by[92][93]:

$$\sigma_{\text{eff}} = \sum_{ij} \sigma(\tilde{\chi}_i \tilde{\chi}_j \rightarrow XY) \times \frac{g_i g_j}{g_{\text{eff}}^2} (1 + \Delta_i)^{3/2} (1 + \Delta_j)^{3/2} \exp[-x(\Delta_i + \Delta_j)] \qquad (2.27)$$

where $\Delta_i \equiv (m_{\tilde{\chi}_i} - m_{\tilde{\chi}_1^0})/m_{\tilde{\chi}_1^0}$, g_i denotes the degrees of freedom for $\tilde{\chi}_i$, and

$$g_{\text{eff}} \equiv \sum_{i=1}^{N} g_i (1 + \Delta_i)^{3/2} \exp(-x\Delta_i). \qquad (2.28)$$

For the parameter space delineated by $\lambda \sim \mathcal{O}(0.1)$ and $\mu_{\text{tot}} > 600\,\text{GeV}$, the GNMSSM predictions on the cross-sections $\sigma(\tilde{\chi}_i \tilde{\chi}_j \rightarrow XY)$ can be approximated by scaling the corresponding MSSM ones with factors $f_{\tilde{\chi}_i \tilde{\chi}_j}$, which are $f_{\tilde{\chi}_1^0 \tilde{\chi}_1^0} = \cos^4 \theta$, $f_{\tilde{\chi}_1^0 \tilde{\chi}_1^\pm} = \cos^2 \theta$, $f_{\tilde{\chi}_3^0 \tilde{\chi}_1^\pm} = \sin^2 \theta$, $f_{\tilde{\chi}_1^0 \tilde{\chi}_2^0} = \cos^2 \theta \sin^2 \theta$, and $f_{\tilde{\chi}_2^0 \tilde{\chi}_1^\pm} = f_{\tilde{\chi}_1^\pm \tilde{\chi}_1^\mp} = 1$. This relationship is verified by calculating the s-wave contributions to the cross-sections for $\tilde{\chi}_1^0 \tilde{\chi}_1^0 \rightarrow WW$ and $\tilde{\chi}_1^0 \tilde{\chi}_1^0 \rightarrow ZZ$, which proceed via t-channel exchanges of $\tilde{\chi}_1^\pm$ and $\tilde{\chi}_1, \tilde{\chi}_2, \tilde{\chi}_3^0$, respectively:

$$\langle \sigma v \rangle_{WW}^s \simeq \frac{1}{128\pi m_{\tilde{\chi}_1^0}^2} g^4 \cos^4 \theta, \quad \langle \sigma v \rangle_{ZZ}^s \simeq \frac{1}{256\pi m_{\tilde{\chi}_1^0}^2} \frac{g^4}{c_W^4} \cos^4 \theta. \qquad (2.29)$$

These results differ from the MSSM predictions[2][94] by a factor $\cos^4 \theta$. It arises from two sources: a $\cos \theta$ scaling of the $\tilde{\chi}_1^0 \tilde{\chi}_1^\pm W$ and $\tilde{\chi}_1^0 \tilde{\chi}_2^0 Z$ couplings, and the strong suppression of $\tilde{\chi}_1^0 \tilde{\chi}_1^0 Z$ and $\tilde{\chi}_1^0 \tilde{\chi}_3^0 Z$ couplings in the GNMSSM.

Overall, these findings demonstrate that both the mass splitting among Higgsino-like particles and the Higgsino-Singlino mixing are crucial in determining the final relic density.

2.5. DM Direct Detection

In scenarios where squarks are extremely massive, the SI scattering of DM off nucleons predominantly arises from the t-channel exchange of CP-even Higgs bosons. The cross-section is given by[2][95][96]

$$\sigma_N^{\mathrm{SI}} = \frac{4\mu_r^2}{\pi} |f^N|^2, \quad f^N = \sum_i^3 f_{h_i}^N = \sum_i^3 \frac{C_{\tilde{\chi}_1^0 \tilde{\chi}_1^0 h_i} C_{NNh_i}}{2m_{h_i}^2}. \tag{2.30}$$

Here, $N = p, n$ denotes a proton (p) or neutron (n), and $\mu_r \equiv m_N m_{\tilde{\chi}_1^0}/(m_N + m_{\tilde{\chi}_1^0})$ represents the reduced mass of the DM–nucleon system. The coupling C_{NNh_i} characterizes the strength of Higgs-nucleon interaction and is written as

$$C_{NNh_i} = -\frac{m_N}{v} \left[F_d^N \left(V_{h_i}^{\mathrm{SM}} - \tan\beta V_{h_i}^{\mathrm{NSM}} \right) + F_u^N \left(V_{h_i}^{\mathrm{SM}} + \frac{1}{\tan\beta} V_{h_i}^{\mathrm{NSM}} \right) \right]. \tag{2.31}$$

In this expression, F_d^N and F_u^N are defined by $F_d^N \equiv f_d^{(N)} + f_s^{(N)} + \frac{2}{27} f_G^{(N)}$ and $F_u^N \equiv f_u^{(N)} + \frac{4}{27} f_G^{(N)}$, where the nucleon form factors $f_q^{(N)} \equiv m_N^{-1} \langle N | m_q q\bar{q} | N \rangle$ for $q = u, d, s$ represent the normalized contribution of light quarks to the nucleon mass. The term $f_G^{(N)} \equiv 1 - \sum_{q=u,d,s} f_q^{(N)}$ accounts for the heavy quarks contributions (see, e.g, Ref. [96][95]). Under the default settings of the microOMEGAs package for $f_q^{(N)}$ [97][98][99], one obtains $F_u^p \simeq F_u^n \simeq 0.15$, $F_d^p \simeq F_d^n \simeq 0.13$, implying that σ_p^{SI} is approximately equal to σ_n^{SI} without strong cancellations between different contributions. This approximate degeneracy, however, is usually broken for small σ_p^{SI} and σ_n^{SI} as suggested by recent LZ results[50].

Regarding the Higgs coupling to the DM pair, $C_{\tilde{\chi}_1^0 \tilde{\chi}_1^0 h_i}$, it is approximated by[70]

$$\begin{aligned} C_{\tilde{\chi}_1^0 \tilde{\chi}_1^0 h_i} \simeq {} & \lambda \sin\theta \cos\theta \left[V_a^{\mathrm{NSM}} (\cos\beta - \sin\beta) + V_a^{\mathrm{SM}} (\cos\beta + \sin\beta) \right] \\ & - \sqrt{2}\kappa V_a^S \sin^2\theta + \frac{\lambda}{\sqrt{2}} V_a^S \cos^2\theta, \end{aligned} \tag{2.32}$$

where the Higgsino-Singlino mixing angle is defined in Eq. (2.24).

In the limit where the charged Higgs bosons are very massive, one finds $V_h^{\mathrm{NSM}} \sim 0$, and $V_{h_s}^{\mathrm{NSM}} \sim 0$. Furthermore, as discussed in Ref. [77], the H-mediated contribution can be safely neglected due to its suppression by a factor $1/m_H^4$. Consequently, assuming $F_u^N = F_d^N$, the SI cross-section can be simplified to[100][101]

$$\sigma_N^{\mathrm{SI}} \simeq 5 \times 10^{-45} \mathrm{cm}^2 \left(\frac{\mathcal{A}}{0.1} \right)^2, \tag{2.33}$$

with

$$\begin{aligned}
\mathcal{A} &= \left(\frac{125\text{GeV}}{m_h}\right)^2 V_h^{\text{SM}} C_{\tilde{\chi}_1^0 \tilde{\chi}_1^0 h} + \left(\frac{125\text{GeV}}{m_{h_s}}\right)^2 V_{h_s}^{\text{SM}} C_{\tilde{\chi}_1^0 \tilde{\chi}_1^0 h_s} \\
&= \lambda(\cos\beta + \sin\beta)\sin\theta\cos\theta\left[\left(\frac{125\text{GeV}}{m_h}\right)^2 (V_h^{\text{SM}})^2 + \left(\frac{125\text{GeV}}{m_{h_s}}\right)^2 \left(V_{h_s}^{\text{SM}}\right)^2\right] \\
&\quad + \frac{\lambda}{\sqrt{2}}\cos^2\theta\left[\left(\frac{125\text{GeV}}{m_h}\right)^2 V_h^{\text{SM}} V_h^S + \left(\frac{125\text{GeV}}{m_{h_s}}\right)^2 V_{h_s}^{\text{SM}} V_{h_s}^S\right] \\
&\quad - \sqrt{2}\kappa\sin^2\theta\left[\left(\frac{125\text{GeV}}{m_h}\right)^2 V_h^{\text{SM}} V_h^S + \left(\frac{125\text{GeV}}{m_{h_s}}\right)^2 V_{h_s}^{\text{SM}} V_{h_s}^S\right].
\end{aligned} \tag{2.34}$$

Given that $V_h^{\text{SM}} \simeq V_{h_s}^S \simeq 1$, $V_h^S \simeq -V_{h_s}^{\text{SM}}$, $\cos\theta \sim 1$, and that $V_h^S, V_{h_s}^{\text{SM}}, \sin\theta$ are proportional to λ, we have the following observations:

- The leading contributions in the first, second, and third terms of $\mathcal{A}$ scale as λ^2, λ^2, and $\kappa\lambda^3$, respectively.

- Cancellations occur among the contributions from different Higgs bosons, with h_s potentially exerting a significant influence when it is light.

- A sufficiently large κ with an appropriate sign can counterbalance the other contributions.

- The sign of V_h^S, as given in Eq. (2.12), can induce cancellation between the first and second terms of $\mathcal{A}$.

On the other hand, the SD scattering cross section is primarily due to t-channel Z boson exchange. It can be expressed as [102]

$$\sigma_N^{\text{SD}} = C_N \times \left(\frac{C_{\tilde{\chi}_1^0 \tilde{\chi}_1^0 Z}}{0.1}\right)^2, \tag{2.35}$$

where $C_n = 3.1 \times 10^{-40}\text{pb}$ and $C_p = 4.0 \times 10^{-40}\text{pb}$ reflect differences in nuclear structure. The normalized coupling of DM to Z boson, $C_{\tilde{\chi}_1^0 \tilde{\chi}_1^0 Z}$, is given by $C_{\tilde{\chi}_1^0 \tilde{\chi}_1^0 Z} \equiv N_{13}^2 - N_{14}^2$. Notably, this coupling vanishes under the mixing angle approximation in Eq. (2.23), reflecting a strong suppression of the SD cross-section. However, using the exact expressions for the neutralino mixing matrix elements given in Eq. (2.21), one obtains

$$C_{\tilde{\chi}_1^0 \tilde{\chi}_1^0 Z} \approx \frac{\mu_{\text{tot}} + m_{\tilde{\chi}_1^0}}{\mu_{\text{tot}}} \frac{\lambda^2 v^2 \cos 2\beta}{\lambda^2 v^2 (1 + \sin 2\beta) + 4(\mu_{\text{tot}} + m_{\tilde{\chi}_1^0})^2}. \tag{2.36}$$

Using the approximation of $m_{\tilde{\chi}_1^0}$ in Eq. (2.20), one can infer that $C_{\tilde{\chi}_1^0 \tilde{\chi}_1^0 Z}$ is suppressed by a factor of $\lambda^2 v^2/(d\mu_{\text{tot}}^2)$. It vanishes when $\tan\beta = 1$, which was called the blind-spot for the SD scattering in literatures.

3. Numerical Study

This section outlines our sampling methodology and examines the distinctive features of the Higgsino DM in the GNMSSM. Our numerical analysis follows a systematic approach using state-of-the-art computational tools. We begin by implementing the GNMSSM model routines using SARAH-4.15.3[103][104][105][106]. The particle spectrum and low-energy flavor observables are then computed using SPheno-4.0.5[107][108][109] and FlavorKit[110], respectively. For DM physics observables, we employ MicrOMEGAs-5.0.4[111][112][113][114][115][116][117][118]. The parameter space exploration is conducted using a parallelized version of the MultiNest algorithm[119] within a modified version of EasyScan[120]. This approach efficiently identifies high-likelihood regions, detects multiple modes, and provides robust Bayesian evidence estimates. To identify viable parameter regions and extract physical insights, we analyze the obtained samples using profile likelihood (PL) methods within the Frequentist statistical framework[121]. In our analysis, we also integrate the latest $125 GeV$ Higgs data and findings from the LZ dark matter direct detection experiment to investigate their impact on the model's characteristics.

Parameter	Prior	Range	Parameter	Prior	Range
κ	Flat	-0.7−0.7	$\tan\beta$	Flat	5−30
λ	Flat	0−0.5	d'	Flat	0.1−0.7
δ	Flat	-0.2−0.2	m_B/TeV	Flat	0.05−0.3
A_t/TeV	Flat	2.5−5	$\mu_{\mathrm{tot}}/\mathrm{TeV}$	Flat	0.6−1.1

Table 1. Parameter space explored in this study, where d' is defined as $d \equiv d/0.1$ for simplicity. All input parameters are assigned flat distributions in their priors due to their well-defined physical interpretations. To concentrate on the effects of Higgsino-Singlino mixing on the DM properties and also to evade strong constraints from the LZ experiment, we set the gaugino masses M_1 and M_2 at 2 TeV to ensure that the Higgsino-Gaugino mixing remains small. Additionally, since the soft trilinear coefficients for the third-generation squarks, A_t and A_b, can significantly influence the SM-like Higgs boson mass through radiative corrections, we establish $A_t = A_b$ and allow them to vary. All other dimensional SUSY parameters not central to the analysis are kept fixed: $\xi' = 0$, $m_C = 400\,\mathrm{GeV}$, $v_s = 600\,\mathrm{GeV}$, and a universal value of 3 TeV for the remaining parameters, consistent with constraints from the LHC new physics searches. All parameters are defined at the renormalization scale $Q_{\mathrm{input}} = 1\,\mathrm{TeV}$. The final parameter space is derived through multiple scans over significantly wider ranges.

3.1. Research Strategy

Through a process of trial and error, we identify the GNMSSM parameter space to be explored, as shown in Table 1. Given the high degree of fine-tuning in the Higgsino DM region, we partition the $\lambda - \mu_{\mathrm{tot}}$ plane into a 10×10 grid to capture the underlying subtle physics more accurately. Each grid subsection undergoes a parallelized MultiNest scan with 6000 live points, configured by setting the parameter of the algorithm, $nlive$, at 6000.

During these scans, we construct a joint likelihood function that incorporates DM relic density, DM direct detection limits, and a range of other experimental constraints, including LHC Higgs data. For the relic density likelihood $\mathcal{L}_{\Omega h^2}$, we adopt a Gaussian distribution centered on the Planck collaboration's measurement[1], with a 10% theoretical uncertainty to account for systematic calculation errors. For direct detection constraints from the LZ results in 2022[49], we define $\mathcal{L}_{\mathrm{LZ}}$ using a Gaussian distribution centered at zero with variance $\delta_\sigma^2 = (\mathrm{UL}_\sigma/1.64)^2 + (0.2\sigma)^2$, where UL_σ represents the 90% confidence-

level upper limit on the SI scattering cross-section, and the 0.2σ term accounts for nuclear response and other theoretical uncertainties[122]. Furthermore, since the SI cross-section for DM–proton scattering, σ_p^{SI}, may significantly deviate from that for DM–neutron scattering, σ_n^{SI}, when the scattering rates are tiny, we define the effective SI cross-section as $\sigma_{\mathrm{eff}}^{\mathrm{SI}} = 0.169\sigma_p^{\mathrm{SI}} + 0.347\sigma_n^{\mathrm{SI}} + 0.484\sqrt{\sigma_p^{\mathrm{SI}}\sigma_n^{\mathrm{SI}}}$[123], which averages the abundance of different xenon isotopes in nature[124], and compare it with the published results of the LZ experiment.

The complete likelihood function is formulated as

$$
\begin{aligned}
\mathcal{L} &\equiv \mathcal{L}_{\Omega h^2} \times \mathcal{L}_{\mathrm{LZ}} \times \mathcal{L}_{\mathrm{Const}}, \\
\mathcal{L}_{\Omega h^2} &= \mathrm{Exp}\left[-\frac{1}{2}\left(\frac{\Omega h^2 - 0.120}{0.012}\right)^2\right], \quad \mathcal{L}_{\mathrm{LZ}} = \mathrm{Exp}\left[-\frac{\sigma_{\mathrm{eff}}^{\mathrm{SI}}}{2\delta_\sigma^2}\right], \\
\mathcal{L}_{\mathrm{Const}} &= \begin{cases} 1, & \text{Satisfying all experimental constraints} \\ \mathrm{Exp}[-100]. & \text{Otherwise} \end{cases}
\end{aligned}
\tag{3.1}
$$

Constraints included in $\mathcal{L}_{\mathrm{Const}}$ encompass:

- **DM component:** $\tilde{\chi}_1^0$ should be Higgsino-dominated, i.e., $\sqrt{N_{13}^2 + N_{14}^2} > 0.5$.

- **Higgs data fit:** The properties of the Higgs boson h observed at the LHC must align with ATLAS and CMS measurements at 95% confidence level. Assuming a $3 GeV$ combined theoretical and experimental uncertainty for m_h, we computed the p-value of the fit using `HiggsSignals-2.6.2`[125][126][127][128] and required it larger than 0.05.

- **Extra Higgs searches:** Comprehensive searches for additional Higgs bosons at LEP, Tevatron, and LHC are implemented using `HiggsBounds-5.10.2`[129][130][131][132][133].

- **Indirect DM searches:** The Fermi-LAT collaboration has made years of observations of dwarf galaxies, limiting the annihilation cross section as a function of the DM mass. We employed the likelihood function proposed in Ref.[134]{m/137/} to implement this constraint. We also used the latest MDHAT package, which incorporated 14 years of publicly available Fermi-LAT data from a set of 54 dwarf spheroidal galaxies, to improve this constraint[135][136].

- B-**physics observables:** Branching ratios for $B_s \to \mu^+\mu^-$ and $B \to X_s\gamma$ must conform to experimental measurements within 2σ[137].

Notably, we exclude LHC SUSY search constraints as they do not impact our parameter space due to the high mass of the Higgsino DM under consideration.
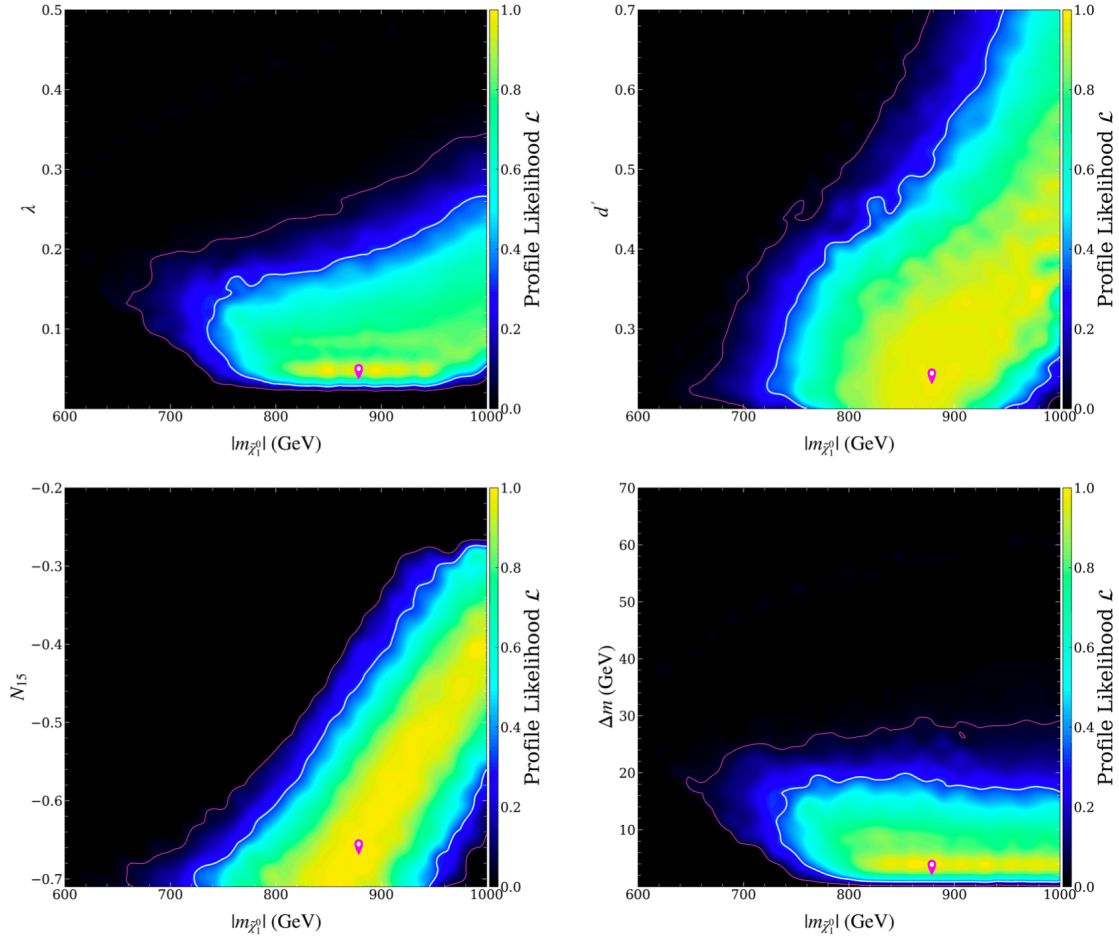
Figure 1. Two-dimensional profile likelihoods of the function $\mathcal{L}$ in Eq. (3.1), projected onto the $|m_{\tilde{\chi}_1^0}| - \lambda$, $|m_{\tilde{\chi}_1^0}| - d'$, $|m_{\tilde{\chi}_1^0}| - N_{15}$, and $|m_{\tilde{\chi}_1^0}| - \Delta m$ planes, respectively. Here, $N_{15} \simeq \sin\theta$ represents the fraction of Singlino component in the Higgsino-dominated DM, and $\Delta m \equiv m_{\tilde{\chi}_1^\pm} - |m_{\tilde{\chi}_1^0}|$ denotes the mass splittings between $\tilde{\chi}_1^\pm$ and $\tilde{\chi}_1^0$. Since the best point (marked with pin symbol) yields $\chi^2 \simeq 0$, the boundaries for 1σ and 2σ confidence intervals correspond to $\chi^2 \simeq 2.3$ and $\chi^2 \simeq 6.18$, respectively, indicated by white and red solid lines. This figure illustrates how the DM relic abundance constrains the parameter space of the GNMSSM.

3.2. Numerical Results

Through our scanning procedure, we obtained a total of 2,146,266 parameter points. Based on these points, we plotted the PL distributions across various two-dimensional planes[1], enabling us to analyze the characteristics of Higgsino DM and its underlying physical mechanisms.

We first examine how the DM relic abundance depends on the model parameters. Analysis of the scanned parameter points reveals that in most cases, DM achieves the experimentally measured relic abundance

primarily through co-annihilation processes $\tilde{\chi}_1^0 \tilde{\chi}_1^\pm, \tilde{\chi}_2^0 \tilde{\chi}_1^\pm \to XY$, where X and Y denote SM particles, along with the annihilation process $\tilde{\chi}_1^0 \tilde{\chi}_1^0 \to ZZ, WW, t\bar{t}$. According to the relevant equations in section 2.4 for very massive gaugino cases, the relic density primarily depends on the mixing angle θ with $\sin\theta \simeq N_{15}$ and mass splitting $\Delta m \equiv m_{\tilde{\chi}_1^\pm} - |m_{\tilde{\chi}_1^0}|$, which are ultimately determined by parameters λ, $\mu_{tot} \simeq |m_{\tilde{\chi}_1^0}|$, and d'. Fig. 1 shows the PL distribution of the parameter points projected onto the $|m_{\tilde{\chi}_1^0}| - \lambda$, $|m_{\tilde{\chi}_1^0}| - d'$, $|m_{\tilde{\chi}_1^0}| - N_{15}$, and $|m_{\tilde{\chi}_1^0}| - \Delta m$ planes, where white and red solid lines represent the boundaries of 1σ and 2σ confidence intervals, respectively. Given that the best-fit point has $\chi^2 \simeq 0$, these contour lines correspond to $\chi^2 \simeq 2.3$ and $\chi^2 \simeq 6.18$, respectively. From Fig. 1, we can draw the following conclusions:

- In the Higgsino DM scenario of the GNMSSM, due to mixing between Higgsino and Singlino, DM with mass as low as 650GeV can yield a relic density consistent with the experimental measurements. In contrast, the Higgsino DM in the MSSM requires a mass of approximately 1.1TeV to obtain an appropriate relic density, with a typical Δm value of less than 1GeV after considering the constraints from latest LZ results (see point P2 in Table 2). This indicates that GNMSSM has a significantly larger parameter space for producing viable Higgsino DM than the MSSM.

- When DM mass is around 650GeV, relatively large values of $|N_{15}|$ and Δm (specifically $N_{15} \simeq -0.70$, $\Delta m \simeq 20$GeV) are required to match experimental results. This is because under these conditions, the effective annihilation cross-section of DM can be significantly lower than that predicted by the MSSM for the same mass, thereby increasing the relic density.

- As $|m_{\tilde{\chi}_1^0}|$ gradually increases, the 2σ upper limits of λ, d', and N_{15} all rise significantly, from 0.12, 0.05, and -0.7 to 0.35, 0.7, and -0.25, respectively. This occurs because as $|m_{\tilde{\chi}_1^0}|$ increases, DM can achieve the experimentally measured relic abundance through the co-annihilation of Higgsino-dominated particles alone, making the mixing between Higgsino and Singlino no longer a necessary condition for predicting the correct relic density. Consequently, the relic density's dependence on N_{15} weakens, allowing it to vary over a wider range (for instance, $-0.6 \lesssim N_{15} \lesssim -0.25$ when the DM mass is 1000 GeV). According to Eq. (2.24), both λ and d' can take larger values in this case. In comparison, as $|m_{\tilde{\chi}_1^0}|$ increases from 700 GeV, the 2σ upper limit of Δm shows only a slight increase, stabilizing around 25 GeV. This behavior arises because Δm appears only in the exponential term of σ_{eff} in Eq. (2.27). If we perform a Taylor expansion of Eq. (2.27), the leading-order contribution of the co-annihilations to σ_{eff}, usually acting as the dominant component of the total cross-section, is

approximately independent of DM mass. This fact suggests that the relic density and its related Δm are also largely independent of DM mass.
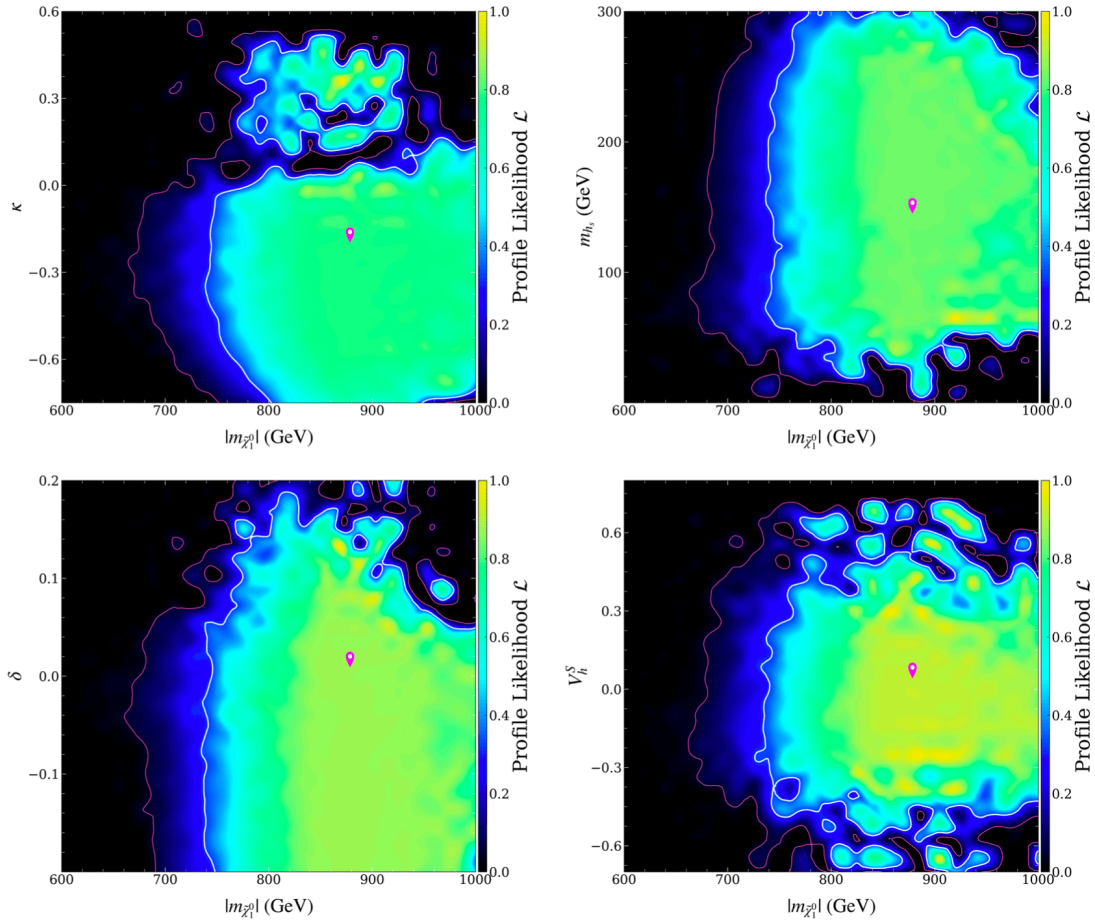
Figure 2. Same as Fig. 1, but for the profile likelihood projected onto the $|m_{\tilde{\chi}_1^0|} - \kappa$, $|m_{\tilde{\chi}_1^0|} - m_{h_s}$, $|m_{\tilde{\chi}_1^0|} - \delta$, and $|m_{\tilde{\chi}_1^0|} - V_h^S$ planes, respectively.

- The yellow regions in Fig. 1 correspond to relatively small χ^2 values, indicating that these areas can well explain experimental results. The PL map on the $|m_{\tilde{\chi}_1^0|} - \lambda$ plane shows that λ in this region is concentrated within a narrow range. This is because λ not only affects DM relic density through N_{15} and Δm, but also influences Higgs physics (see the Higgs mass matrix in Eq. (2.7)) and DM–nucleon scattering in more complex ways. As a result, λ is a critical parameter strongly constrained by various experiments, with current LZ experimental results favoring tiny λ values. Fig. 1 also shows that d' and N_{15} can span a wider ranger, reflecting the fact that, for larger DM masses, neither d' nor N_{15} is crucial to DM physics. Moreover, Δm is similarly confined to a narrow range in the figure. This

is because Δm affects the relic density exponentially, and large variations in Δm would lead to rapid changes in the relic abundance, which contradicts experimental results.

Next, we discuss how direct detection experiments constrain the parameter space. From Eq. (2.34), we know that the SI scattering cross-section between DM and nucleons depends on parameters λ, N_{15}, κ, m_{h_s}, and V_h^S. Fig. 2 depicts the PL distributions for the $m_{\tilde{\chi}_1^0} - \kappa$, $m_{\tilde{\chi}_1^0} - m_{h_s}$, $m_{\tilde{\chi}_1^0} - \delta$, and $m_{\tilde{\chi}_1^0} - V_h^S$ planes, where parameter δ influences V_h^S through Eq. (2.12). The results show that κ, m_{h_s}, δ, and V_h^S can vary across relatively large regions, primarily due to two reasons:

- Eq. (2.34) indicates that the leading-order contribution to the SI scattering cross section is proportional to λ^4. When λ is sufficiently small, the cross-section can be drastically reduced, ensuring compatibility with the LZ experiment and allowing other parameters to be larger.

- Depending on the signs of N_{15}, κ, and V_h^S, different terms in Eq. (2.34) may cancel each other, further reducing the scattering cross-section between DM and nucleons. When κ takes large values and h_s is light, the influence of the singlet-dominated Higgs particle on the scattering cross-section increases, which can further enhances this cancellation effect. Combining the results from Fig. 1 and Fig. 2, one sees that negative values of N_{15}, κ, δ, and V_h^S tend to strengthen these cancellations, thus aligning more easily with LZ experimental results.

Furthermore, we found that since the SD scattering cross-section between DM and nucleons is suppressed, its constraints on the parameter space are generally weaker compared to SI scattering when considering the LZ data in 2022. However, in certain special cases, it may also provide more stringent constraints.
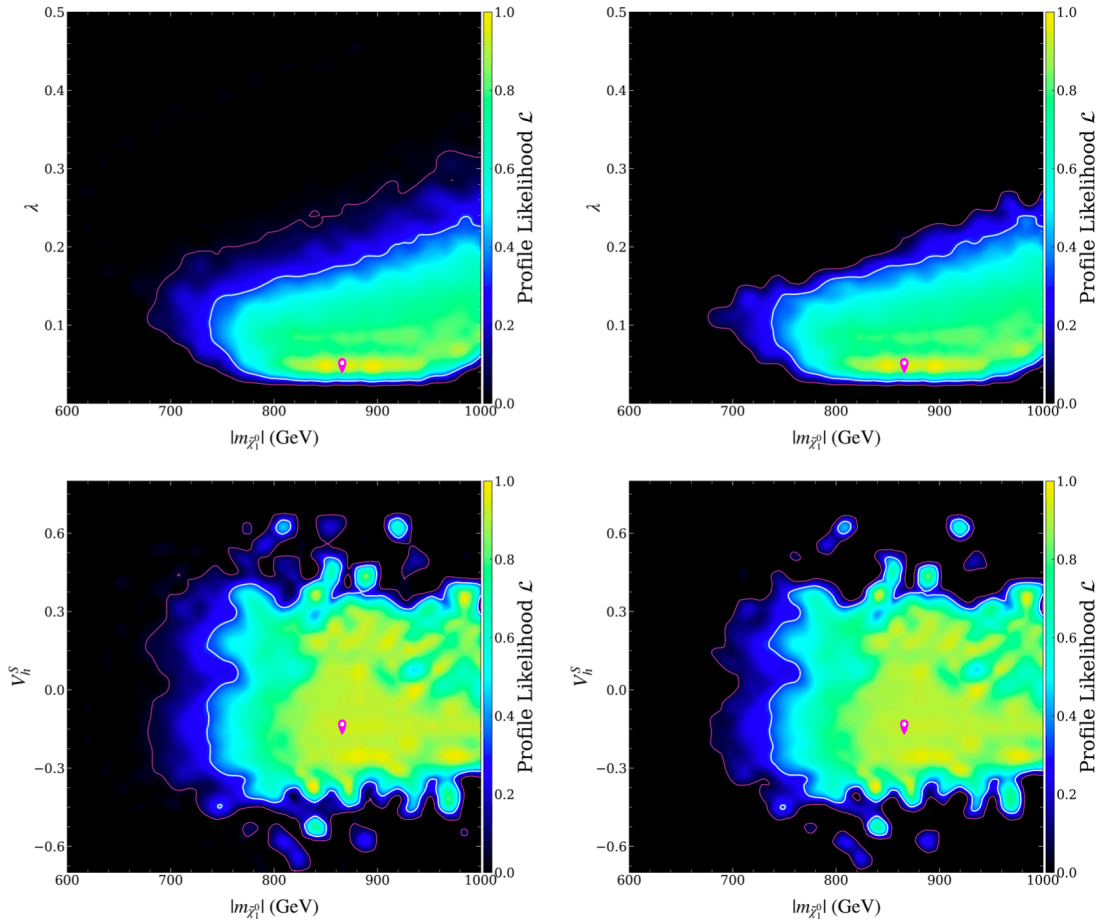
Figure 3. Profile likelihood maps of $\mathcal{L}$, projected onto the $\left|m_{\tilde{\chi}_1^0}\right| - \lambda$ planes (upper panels) and the $\left|m_{\tilde{\chi}_1^0}\right| - V_h^S$ planes (bottom panels). The left panels show results after refitting the original scan samples to the updated Higgs data, while the right panels include additional constraints from the latest LZ experimental results. This comparison illustrates the progressive impact of each experimental constraint set on the viable parameter space.

4. Improved Constraints

The continued operation of the LHC has produced a substantial amount of $125\,\mathrm{GeV}$ Higgs boson data, enabling increasingly precise measurements of its properties[86][87]. In parallel, the LZ experiment recently released new DM search results, improving its DM–nucleon scattering sensitivity by nearly one order of magnitude when compared to the results in 2022[50]. These advances provide an opportunity to impose more stringent constraints on the GNMSSM.

To capitalize on these updated measurements, we refined the Higgs data fitting in Sec. 3 using `HiggsTools-1.2`, the latest version of `HiggsTools`[138], and reanalyzed the previously scanned parameter points. This updated version of the `HiggsSignals` and `HiggsBounds` represents a significant advancement over `HiggsSignals-2.6.2` by introducing 22 additional physical observables, thereby raising the total number of observables for fitting Higgs properties to 129[138]. In our refitting process, we assumed an uncertainty of $3\,\mathrm{GeV}$ for m_h and required the samples to satisfy $\chi^2_{\mathrm{Higgs}} - \chi^2_{\mathrm{SM},125} \lesssim 6.18$, where χ^2_{Higgs} is the value obtained from the $125\,\mathrm{GeV}$ Higgs data fit with `HiggsTools-1.2`, and $\chi^2_{\mathrm{SM},125} \simeq 176.3$ corresponds to a pure SM Higgs boson in the GNMSSM[76]. Additionally, we incorporated the latest LZ results to further constrain the DM property, which is the focus of this work.
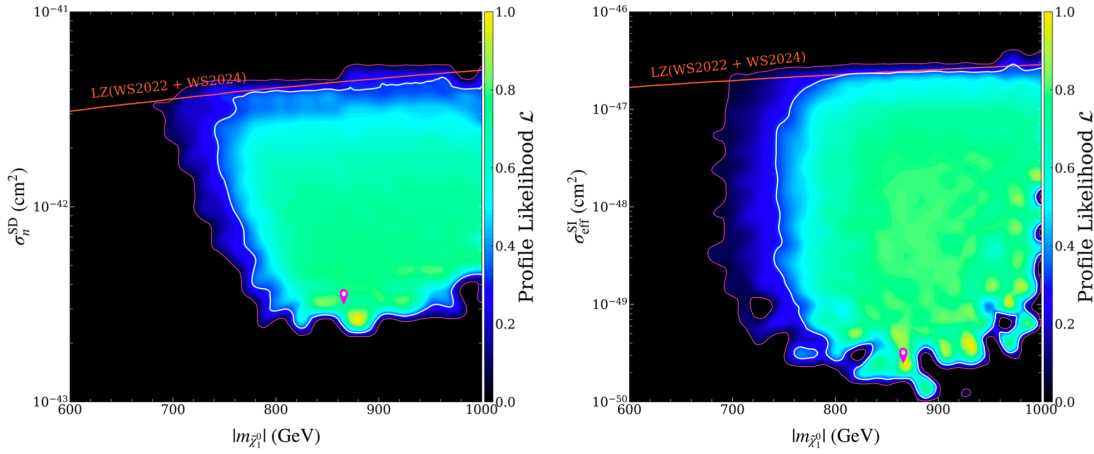
Figure 4. Profile likelihoods of σ_n^{SD} and $\sigma_{\mathrm{eff}}^{\mathrm{SI}}$ as functions the DM mass. All displayed points satisfy the complete set of updated experimental constraints, reflecting current status of DM interactions with nucleon in the GNMSSM.

Point P1			Point P2	
Parameter	Value		Parameter	Value
$\tan\beta$	21.96		$\tan\beta$	29.86
λ, κ	$0.037, -0.13$		λ, κ	$0.009, -0.029$
d', δ	$0.21, -0.10$		d', δ	$1.80, 0.17$
v_s, μ_{tot}	$600.0, 853.2$		v_s, μ_{tot}	$600.0, 1115.2$
m_A, m_B, m_C	$3000, 194.3, 400$		m_A, m_B, m_C	$3000, 135.4, 400$
M_1, M_2	$2000, 2000$		M_1, M_2	$6000, 6000$
Particle	Mass spectrum		Particle	Mass spectrum
$\tilde\chi_1^0, \tilde\chi_2^0, \tilde\chi_3^0$	$-865.9, 866.1, -875.5$		$\tilde\chi_1^0, \tilde\chi_2^0, \tilde\chi_3^0$	$1136.9, -1137.3, -1316.1$
$\tilde\chi_4^0, \tilde\chi_5^0$	$2007.4, 2023.3$		$\tilde\chi_4^0, \tilde\chi_5^0$	$5940.1, 6064.5$
$\tilde\chi_1^\pm, \tilde\chi_2^\pm$	$868.2, 2023.2$		$\tilde\chi_1^\pm, \tilde\chi_2^\pm$	$1137.5, 5940.2$
h_s, h, H	$148.6, 124.6, 3242.2$		h_s, h, H	$116.2, 124.5, 4242.8$
Rotation matrix	Element value		Rotation matrix	Element value
$V_{h_s}^S, V_{h_s}^{SM}, V_h^S, V_h^{SM}$	$-98, 17, -17, -98$		$V_{h_s}^S, V_{h_s}^{SM}, V_h^S, V_h^{SM}$	$96, -25, 24, 96$
$N_{11}, N_{12}, N_{13}, N_{14}, N_{15}$	$-1, 1, 50, 51, -70$		$N_{11}, N_{12}, N_{13}, N_{14}, N_{15}$	$1, -1, 71, -70, 0$
$N_{21}, N_{22}, N_{23}, N_{24}, N_{25}$	$-3, 5, -71, 71, 0$		$N_{21}, N_{22}, N_{23}, N_{24}, N_{25}$	$0, -1, -71, -71, -1$
$N_{31}, N_{32}, N_{33}, N_{34}, N_{35}$	$1, -1, -50, -50, -71$		$N_{31}, N_{32}, N_{33}, N_{34}, N_{35}$	$0, 0, 1, -4, 99$
$N_{41}, N_{42}, N_{43}, N_{44}, N_{45}$	$-47, -88, -1, 3, 0$		$N_{41}, N_{42}, N_{43}, N_{44}, N_{45}$	$0, 99, 0, -1, 0$
$N_{51}, N_{52}, N_{53}, N_{54}, N_{55}$	$88, -47, -2, 5, 0$		$N_{51}, N_{52}, N_{53}, N_{54}, N_{55}$	$-99, 0, 0, -1, 0$
Primary annihilation	Fraction [%]		Primary annihilation	Fraction [%]
$\tilde\chi_2^0\tilde\chi_1^\pm \to d\bar{u}/\bar{d}u$	8.40		$\tilde\chi_1^0\tilde\chi_2^0 \to t\bar{t}$	6.90
$\tilde\chi_2^0\tilde\chi_1^\pm \to s\bar{c}/\bar{s}c$	8.40		$\tilde\chi_1^0\tilde\chi_1^\pm \to u\bar{d}/\bar{d}u$	6.73
$\tilde\chi_1^0\tilde\chi_1^\pm \to d\bar{u}/\bar{u}d$	4.36		$\tilde\chi_1^0\tilde\chi_1^\pm \to s\bar{c}/\bar{c}s$	6.73
$\tilde\chi_1^0\tilde\chi_1^\pm \to c\bar{s}/\bar{c}s$	4.36		$\tilde\chi_2^0\tilde\chi_1^\pm \to d\bar{u}/\bar{d}u$	6.43
$\tilde\chi_2^0\tilde\chi_1^\pm \to e\bar{\nu}_e/\bar{\nu}_e e$	2.80		$\tilde\chi_2^0\tilde\chi_1^\pm \to s\bar{c}/\bar{s}c$	6.43

Point P1			Point P2	
Parameter	Value		Parameter	Value
$\tilde{\chi}_1^0\tilde{\chi}_1^\pm \to \mu\bar{\nu}_\mu/\bar{\nu}_\mu\mu$	2.80		$\tilde{\chi}_2^+\tilde{\chi}_1^- \to t\bar{t}$	5.41
$\tilde{\chi}_1^+\tilde{\chi}_1^- \to W^+W^-$	2.67		$\tilde{\chi}_2^0\tilde{\chi}_1^\pm \to b\bar{t}/t\bar{b}$	4.34
$\tilde{\chi}_2^0\tilde{\chi}_1^\pm \to \tau\bar{\nu}_\tau/\bar{\nu}_\tau\tau$	2.59		$\tilde{\chi}_1^+\tilde{\chi}_1^- \to b\bar{t}/t\bar{b}$	4.22
DM observable	Value		DM observable	Value
Ωh^2	0.120		Ωh^2	0.118
$\sigma_{p,n}^{SI}/(10^{-50}\mathrm{cm}^2)$	9.67, 0.25		$\sigma_{p,n}^{SI}/(10^{-47}\mathrm{cm}^2)$	2.25, 2.31
$\sigma_{p,n}^{SD}/(10^{-43}\mathrm{cm}^2)$	4.12, 3.14		$\sigma_{p,n}^{SD}/(10^{-45}\mathrm{cm}^2)$	2.67, 2.05

Table 2. Detailed information for two benchmark points compatible with all experimental measurements. Point P1 represents the best-fit point from Fig. 3, while P2 corresponds to the MSSM limit of the GNMSSM, characterized by a particularly small λ value. All mass-dimensional parameters are expressed in GeV, and elements of the rotation matrices V and N are presented in units of 10^{-2}.

Following these refinements, our sample size decreased significantly—from the original dataset of 2,146,266 samples to 276,077 samples when applying only the updated Higgs data constraints, and further to 30,299 samples when incorporating both updated constraints. This substantial reduction demonstrates the remarkable power of recent experimental advancements in constraining the viable parameter space. However, despite these stringent constraints, most of the two-dimensional PL maps in Fig. 1 and Fig. 2 remained largely unchanged, with notable exceptions occurring only in the $|m_{\tilde{\chi}_1^0}| - \lambda$ and $|m_{\tilde{\chi}_1^0}| - V_h^S$ planes. This selective sensitivity highlights a key insight into the model: among all parameters, λ and V_h^S alone play particularly crucial roles in Higgs and DM phenomenology.

To illustrate clearly the impacts of these new experimental results, we present in Fig. 3 the PL maps of $\mathcal{L}$, projected onto the $|m_{\tilde{\chi}_1^0}| - \lambda$ and $|m_{\tilde{\chi}_1^0}| - V_h^S$ planes. The left panels display results obtained after refitting the original scan samples to the updated Higgs data, while the right panels include the additional constraints from the latest LZ experimental results. The upper panels demonstrate that the 2σ upper bound on λ decreases from approximately 0.35 in Fig. 1 to 0.32 (left panel) and further to

0.28 (right panel). Interestingly, the most favored region for λ, highlighted by the yellow band, remains stable around 0.04, consistent with our previous findings. Turning to V_h^S, the allowed region contracts significantly, particularly near the boundaries, as clearly demonstrated by comparing the bottom–right panel of Fig. 2 with the bottom panels of Fig. 3. Moreover, even under the circumstance of these increasingly stringent constraints, our analysis reveals that the DM can still be as light as approximate 660GeV while fully compatible with all experimental measurements.

We also present in Fig.4 the PL map of $\mathcal{L}$ on the $|m_{\tilde{\chi}_1^0}| - \sigma_n^{SD}$ and $|m_{\tilde{\chi}_1^0}| - \sigma_{\mathrm{eff}}^{SI}$ planes, considering all samples that satisfy the updated constraints. For reference, the latest LZ exclusion bounds from Ref. [50] are also shown. It can be seen that σ_n^{SD} can be reduced to about $2 \times 10^{-43} \mathrm{cm}^2$ for $\lambda \simeq 0.02$, roughly one order of magnitude below the current LZ limits. Even more dramatically, $\sigma_{\mathrm{eff}}^{SI}$ can reach values as low as $10^{-50} \mathrm{cm}^2$, which lies three orders of magnitude below the corresponding LZ limits and two orders of magnitude below the neutrino floor. The reason behind these disparities is that as indicated by Eq. (36), σ_n^{SD} is suppressed only by a factor of $\lambda^4 v^4/(d^2 \mu_{\mathrm{tot}}^4)$, whereas $\sigma_{\mathrm{eff}}^{SI}$ depends on multiple parameters of the GNMSSM, each contribution being suppressed by at least λ^4 with the added possibility of cancellations among different terms. Our analysis further indicates important implications for future experiments: if upcoming DM direct detection experiments improve current sensitivities by just one order of magnitude without finding any evidence of DM, the parameter λ would be constrained to values significantly smaller than 0.02. This constraint would primarily arise from limitations on σ_n^{SD} rather than on $\sigma_{\mathrm{eff}}^{SI}$. Consequently, the Bayesian evidence for the Higgsino DM scenario within the GNMSSM framework would be substantially reduced.

Finally, we present in Table 2 detailed information for two benchmark points that satisfy all experimental constraints. Point P1 corresponds to the best-fit point obtained by minimizing the χ^2 function specified in footnote 1. It features substantial Higgsino-Singlino mixing, enabling a sub-TeV $\tilde{\chi}_1^0$ to achieve the measured DM relic abundance primarily through co-annihilation processes involving Higgsino-dominated states. By contrast, point P2 represents the MSSM limit within the GNMSSM framework, illustrating a viable pure Higgsino DM scenarios. It is characterized by an extremely small λ, which explicitly suppresses the Higgsino–Singlino mixing. This fundamental difference in mixing significantly alters the relative importance of various annihilation channels in the two scenarios. For instance, when examining the effective annihilation cross-section σ_{eff} formulated in Eq. (2.27), we find that the $\tilde{\chi}_1^0 \tilde{\chi}_2^0 \to t\bar{t}$ process contributes only 1.1% to σ_{eff} for Point P1, whereas this contribution

increases to 6.9% for Point P2. Consequently, a heavier $\tilde{\chi}_1^0$ mass of approximately 1.1 TeV is required for Point P2 to attain the correct relic abundance via Higgsino co-annihilation mechanisms.

Aside from these evident differences, another crucial distinction between the two points lies in the gaugino masses: M_1 and M_2 in P1 are significantly smaller than those in P2, yet both configurations remain compatible with LZ results. This compatibility arises because the effects of Higgsino–Singlino mixing on DM–nucleon scattering cross-sections can effectively cancel against those from Gaugino–Higgsino mixing, allowing for relatively light gauginos around 2 TeV to remain consistent with the direct detection constraints. To illustrate the importance of this cancellation mechanism, consider that if we set $M_1 = M_2 = 2$ TeV while keeping other parameters of P2 unchanged, the predicted cross-sections would increase drastically: $\sigma_p^{SI} = 6.8 \times 10^{-46}$ cm^2, $\sigma_n^{SI} = 7.0 \times 10^{-46}$ cm^2, $\sigma_p^{SD} = 4.7 \times 10^{-43}$ cm^2, and $\sigma_n^{SD} = 3.6 \times 10^{-43}$ cm^2. All of these values exceed current LZ upper bounds by more than one order of magnitude. These findings underscore the central conclusion of this work: the GNMSSM provides a significantly broader and more flexible parameter space than the MSSM for accommodating viable Higgsino-dominated DM scenarios.

5. Conclusion

Higgsino DM represents a compelling candidate within supersymmetric frameworks, offering a unique convergence of theoretical insight and experimental motivations. While the MSSM traditionally positioned Higgsino DM at around 1 TeV to achieve the correct relic density, we showed that there still exist viable parameter regions in the GNMSSM with Higgsino DM at significantly lower masses via mixing with Singlino, even confronting with current severe LZ constraints.

We performed a comprehensive analysis of the GNMSSM, focusing on the Higgsino–dominated neutralino as a DM candidate. Our study systematically explored the parameter space by incorporating a range of experimental constraints, including the latest 125 GeV Higgs data and the LZ results in 2024. Our analysis revealed the following key findings:

- **Lower than 1 TeV Higgsino DM**

  In the GNMSSM, Higgsino-dominated neutralinos can achieve the correct DM relic density at significantly lower masses at approximately 660 GeV, which is substantially below the 1 TeV threshold typical in the MSSM. This feature is facilitated by the Higgsino-Singlino mixing, which can produce

correct relic density without invoking extensive Higgsino-gaugino mixing that would otherwise compromise direct detection compatibility.

- **Lower DM-nucleon scattering rate**

  Despite the increasingly stringent constraints from experiments like LZ, the GNMSSM maintains a considerable viable parameter space. This robustness stems from the Higgsino-Singlino mixing, which can effectively suppress the SI scattering cross-sections.

- **Moderate cancellations**

  In order to satisfy the relic density and direct detection constraints, parameter λ has to keep at a low value of $\mathcal{O}(0.1)$. This set a lower SI scattering cross-section globally first, then other parameters like κ and V_h^S can be tuned to satisfy the direct detection constraints. This reflects cancellations among different terms in the SI amplitude.

In summary, our analysis indicates that the GNMSSM presents a viable alternative to the MSSM, offering refined strategies to tackle persistent challenges in supersymmetric DM models. By incorporating additional degrees of freedom from the singlet sector, we demonstrate how theoretical constraints can be effectively addressed while ensuring phenomenological consistency. Our results underscore the potential of the GNMSSM to provide a compelling framework for Higgsino DM, offering a promising avenue for future experimental searches.

Acknowledgements

Footnotes

[1] In frequentist statistics, the two-dimensional PL refers to the maximum likelihood value in a specific parameter space[121]. For a given set of input parameters $\Theta \equiv (\Theta_1, \Theta_2, \cdots)$, this PL is obtained by maximizing the likelihood function while varying the other parameters:

$$\mathcal{L}(\Theta_A, \Theta_B) = \max_{\Theta_1, \cdots, \Theta_{A-1}, \Theta_{A+1}, \cdots, \Theta_{B-1}, \Theta_{B+1}, \cdots} \mathcal{L}(\Theta), \qquad (3.2)$$

At a given point (Θ_A, Θ_B), $\mathcal{L}(\Theta_A, \Theta_B)$ reflects its capability to explain the experimental data, or alternatively, the data's preference for the parameter space of the theory. Correspondingly, one may

define χ^2 for the PL function as $\chi^2(\Theta_A, \Theta_B) \equiv -2\ln\mathcal{L}(\Theta_A, \Theta_B)$ to measure the point's capability in explaining the data.

References

1. a, b*Aghanim N, Planck collaboration (2020). "Planck 2018 results. VI. Cosmological parameters". Astron. Astrophys.. 641: A6. doi:10.1051/0004-6361/201833910. arXiv:1807.06209. [Erratum: Astron.Astrophys. 652, C4 (2021)].*

2. a, b, c, d*Jungman G, Kamionkowski M, Griest K (1995). "Supersymmetric dark matter". Physics Reports. 333 (s 5–6): 167–182.*

3. △*Kane GL, Wells JD (1996). "Higgsino Cold Dark Matter Motivated by Collider Data". Physical Review Letters. 76 (24): 4458–4461. doi:10.1103/PhysRevLett.76.4458. arXiv:hep-ph/9603336.*

4. △*Drees M, Nojiri MM, Roy DP, Yamada Y (1997). "Light Higgsino Dark Matter". Physical Review D. 56 (1): 276–290. doi:10.1103/PhysRevD.56.276. hep-ph/9701219.*

5. △*Masip M, Mastromatteo I (2006). "Higgsino Dark Matter in Partly Supersymmetric Models". Physical Review D. 73 (1): 015007. doi:10.1103/PhysRevD.73.015007. arXiv:hep-ph/0510311.*

6. △*Wang F, Wang W, Yang JM (2006). "Dark Matter Constraints on Gaugino/Higgsino Masses in Split Supersymmetry and Their Implications at Colliders". The European Physical Journal C. 46 (2): 521–526. doi:10.1140/epjc/s2006-02522-x. arXiv:hep-ph/0512133.*

7. △*Hall JP, King SF (2009). "Neutralino Dark Matter with Inert Higgsinos and Singlinos". Journal of High Energy Physics. 08 (08): 088. doi:10.1088/1126-6708/2009/08/088. arXiv:0905.2696.*

8. △*Sinha K (2013). "Higgsino Dark Matter and the Cosmological Gravitino Problem". AIP Conf. Proc.. 1534 (1): 146–155. doi:10.1063/1.4807352. arXiv:1212.0011 [hep-ph].*

9. △*Mayes VE, Lutz AW (2015). "Light Higgsino Dark Matter in the MSSM on D-branes". Journal of Physics G: Nuclear and Particle Physics. 42 (9): 095006. doi:10.1088/0954-3899/42/9/095006. arXiv:1412.1452.*

10. a, b*Kowalska K, Sessolo EM (2018). "The Discreet Charm of Higgsino Dark Matter - a Pocket Review". Adv. High Energy Phys.. 2018 (1): 6828560. doi:10.1155/2018/6828560. arXiv:1802.04097.*

11. a, b, c*Delgado A, Quirós M (2021). "Higgsino Dark Matter in the MSSM". Phys. Rev. D. 103 (1): 015024. doi:10.1103/PhysRevD.103.015024. arXiv:2008.00954.*

12. △*Wang K, Zhu J (2024). "Investigating Higgsino Dark Matter in the Semi-Constrained NMSSM". Chinese Physics C. 48 (11): 113101. doi:10.1088/1674-1137/ad6e60. arXiv:2406.15939.*

13. ^*Evans JL, Olive KA (2022). "Higgsino Dark Matter in Pure Gravity Mediated Supersymmetry". Physical Review D. **106** (5): 055026. doi:10.1103/PhysRevD.106.055026. arXiv:2202.07830.*

14. ^*Nilles HP (1984). "Supersymmetry, Supergravity and Particle Physics". Phys. Rept.. **110**: 1–162. doi:10.1016/0370-1573(84)90008-5.*

15. ^*Haber HE, Kane GL (1985). "The Search for Supersymmetry: Probing Physics Beyond the Standard Model". Phys. Rept.. **117**: 75–263. doi:10.1016/0370-1573(85)90051-1.*

16. ^*Gunion JF, Haber HE (1986). "Higgs Bosons in Supersymmetric Models. 1." Nucl. Phys. B. **272**: 1. doi:10.1016/0550-3213(86)90340-8. [Erratum: Nucl.Phys.B 402, 567--569 (1993)].*

17. ^*Martin SP (1998). "A Supersymmetry primer". Adv. Ser. Direct. High Energy Phys.. **18**: 1–98. doi:10.1142/9789812839657_0001. hep-ph/9709356.*

18. ^*Ellwanger U, Hugonie C (2018). "The higgsino–singlino sector of the NMSSM: combined constraints from dark matter and the LHC". Eur. Phys. J. C. **78** (9): 735. doi:10.1140/epjc/s10052-018-6204-3. arXiv:1806.09478.*

19. ^*Baer H, Barger V, Sengupta D, Tata X (2018). "Is Natural Higgsino-Only Dark Matter Excluded?" The European Physical Journal C. **78** (10): 838. doi:10.1140/epjc/s10052-018-6306-y. arXiv:1803.11210.*

20. ^*Bae KJ, Baer H, Serce H (2017). "Prospects for Axion Detection in Natural {{SUSY}} with Mixed Axion-Higgsino Dark Matter: Back to Invisible?". Journal of Cosmology and Astroparticle Physics. **06** (06): 024. doi:10.1088/1475-7516/2017/06/024. arXiv:1705.01134.*

21. ^*Baer H (2013). "Radiative Natural Supersymmetry with Mixed Axion/Higgsino Cold Dark Matter". AIP Conf. Proc.. **1534**: 39–46. doi:10.1063/1.4807341. arXiv:1210.7852.*

22. ^*Han C (2019). "Higgsino Dark Matter in a Non-Standard History of the Universe". Phys. Lett. B. **798**: 134997. doi:10.1016/j.physletb.2019.134997. arXiv:1907.09235.*

23. ^*Aoki M, Kubo J, Okawa T, Takano H (2012). "Impact of Inert Higgsino Dark Matter". Physics Letters B. **707** (1): 107–115. doi:10.1016/j.physletb.2011.12.012. arXiv:1110.5403.*

24. ^*Bharucha A, Brümmer F, Ruffault R (2017). "Well-tempered n-plet dark matter". JHEP. **09**: 160. doi:10.1007/JHEP09(2017)160. arXiv:1703.00370.*

25. ^*Kowalska K, Roszkowski L, Sessolo EM, Trojanowski S (2014). "Low fine tuning in the MSSM with higgsino dark matter and unification constraints". JHEP. **04**: 166. doi:10.1007/JHEP04(2014)166. arXiv:1402.1328.*

26. ^*Aparicio L, Cicoli M, Dutta B, Muia F, Quevedo F (2016). "Light Higgsino Dark Matter from Non-thermal Cosmology". JHEP. **11**: 038. doi:10.1007/JHEP11(2016)038. arXiv:1607.00004.*

27. ^*Suryanarayana Mummidi V, Patel KM (2020). "Precision unification and Higgsino dark matter in GUT scale supersymmetry". Phys. Rev. D. **101** (11): 115008. doi:10.1103/PhysRevD.101.115008. arXiv:2001.01505.*

28. a, b*Fox PJ, Kribs GD, Martin A (2014). "Split Dirac Supersymmetry: An Ultraviolet Completion of Higgsino Dark Matter". Phys. Rev. D. **90** (7): 075006. doi:10.1103/PhysRevD.90.075006. arXiv:1405.3692.*

29. ^*Arkani-Hamed N, Dimopoulos S (2005). "Supersymmetric unification without low energy supersymmetry and signatures for fine-tuning at the LHC". JHEP. **06**: 073. doi:10.1088/1126-6708/2005/06/073. arXiv:hep-th/0405159.*

30. ^*Giudice GF, Romanino A (2004). "Split supersymmetry". Nucl. Phys. B. **699**: 65–89. doi:10.1016/j.nuclphysb.2004.08.001. arXiv:hep-ph/0406088. [Erratum: Nucl.Phys.B 706, 487–487 (2005)].*

31. ^*Arkani-Hamed N, Dimopoulos S, Giudice GF, Romanino A (2005). "Aspects of split supersymmetry". Nucl. Phys. B. **709**: 3–46. doi:10.1016/j.nuclphysb.2004.12.026. arXiv:hep-ph/0409232.*

32. a, b, c*Martin SP (2024). "Implications of purity constraints on light Higgsinos". Phys. Rev. D. **109** (9): 095045. doi:10.1103/PhysRevD.109.095045. arXiv:2403.19598 [hep-ph].*

33. ^*Chattopadhyay U, Choudhury D, Drees M, Konar P, Roy DP (2006). "Looking for a Heavy Higgsino LSP in Collider and Dark Matter Experiments". Physics Letters B. **632** (1): 114–126. doi:10.1016/j.physletb.2005.09.088. arXiv:hep-ph/0508098.*

34. ^*Chakraborti M, Chattopadhyay U, Rao S, Roy DP (2015). "Higgsino Dark Matter in Nonuniversal Gaugino Mass Models". Physical Review D. **91** (3): 035022. doi:10.1103/PhysRevD.91.035022. arXiv:1411.4517.*

35. ^*Shafi Q, Tiwari A, Un CS (2023). "Third Family Quasi-Yukawa Unification: Higgsino Dark Matter, NLSP Gluino and All That". Physical Review D. **108** (3): 035027. doi:10.1103/PhysRevD.108.035027. arXiv:2302.02905.*

36. a, b, c*Mummidi VS, Patel KM (2019). "Pseudo-Dirac Higgsino Dark Matter in GUT Scale Supersymmetry". Journal of High Energy Physics. **01** (1): 224. doi:10.1007/JHEP01(2019)224. arXiv:1811.06297.*

37. ^*Baer H, Barger V, Huang P, Tata X (2012). "Natural Supersymmetry: LHC, dark matter and ILC searches". JHEP. **05**: 109. doi:10.1007/JHEP05(2012)109. arXiv:1203.5539.*

38. a, b**ATLAS collaboration** (2024). "SUSY July 2024 Summary Plot Update". ATL-PHYS-PUB-2024-014.

39. ^*Chen Q, Hill RJ (2020). "Direct detection rate of heavy Higgsino-like and Wino-like dark matter". Physics Letters B. **804**: 135364. doi:10.1016/j.physletb.2020.135364. arXiv:1912.07795.*

40. ^*Hi7cylmaz Y, Moretti S (2021). "Characterisation of Dark Matter in Direct Detection Experiments: Singlino Versus Higgsino". Nuclear Physics B. **967**: 115404. doi:10.1016/j.nuclphysb.2021.115404. arXiv:2008.06778.*

41. ^*Wang K, Zhu J, Jie Q (2021). "Higgsino Asymmetry and Direct-Detection Constraints of Light Dark Matter in the NMSSM with Non-Universal Higgs Masses". Chinese Physics C. **45** (4): 041003. doi:10.1088/1674-1137/abe03c. arXiv:2011.12848.*

42. <u>a</u>, <u>b</u>*Chun EJ, Jung S, Park JC (2017). "Very Degenerate Higgsino Dark Matter". Journal of High Energy Physics. **01** (1): 009. doi:<u>10.1007/JHEP01(2017)009</u>. arXiv:<u>1607.04288</u>.*

43. <u>^</u>*Yanagida TT, Yokozaki N (2013). "Bino–Higgsino Mixed Dark Matter in a Focus Point Gaugino Mediation". Journal of High Energy Physics. **11**: 020. doi:<u>10.1007/JHEP11(2013)020</u>. arXiv:<u>1308.0536</u>.*

44. <u>a</u>, <u>b</u>*Co RT, Sheff B, Wells JD (2022). "The Race to Find Split Higgsino Dark Matter". Physical Review D. **105** (3): 035012. doi:<u>10.1103/PhysRevD.105.035012</u>. arXiv:<u>2105.12142</u>.*

45. <u>^</u>*Rinchiuso L, Macias O, Moulin E, Rodd NL, Slatyer TR (2021). "Prospects for Heavy WIMP Dark Matter with CTA: The Wino and Higgsino". Physical Review D. **103** (2): 023011. doi:<u>10.1103/PhysRevD.103.023011</u>. arXiv:<u>2008.00692</u>.*

46. <u>^</u>*Bisal S, Chatterjee A, Das D, Pasha SA (2024). "Radiative Corrections to Aid the Direct Detection of the Higgsino-like Neutralino Dark Matter: Spin-Independent Interactions". Physical Review D. **110** (2): 023043. doi:<u>10.1103/PhysRevD.110.023043</u>. arXiv:<u>2311.09937</u>.*

47. <u>^</u>*PandaX-4T collaboration, Meng Y, et al. (2021). "Dark Matter Search Results from the PandaX-4T Commissioning Run". Phys. Rev. Lett.. **127** (26): 261802. doi:<u>10.1103/PhysRevLett.127.261802</u>. arXiv:<u>2107.13438</u>.*

48. <u>^</u>*XENON collaboration, Aprile E, et al. (2023). "First Dark Matter Search with Nuclear Recoils from the XENONnT Experiment". Phys. Rev. Lett.. **131** (4): 041003. doi:<u>10.1103/PhysRevLett.131.041003</u>. arXiv:<u>2303.14729</u>.*

49. <u>a</u>, <u>b</u>*Aalbers J, LZ collaboration (2023). "First Dark Matter Search Results from the LUX-ZEPLIN (LZ) Experiment". Phys. Rev. Lett.. **131** (4): 041002. doi:<u>10.1103/PhysRevLett.131.041002</u>. arXiv:<u>2207.03764</u>.*

50. <u>a</u>, <u>b</u>, <u>c</u>, <u>d</u>*Aalbers J, LZ collaboration (2024). "Dark Matter Search Results from 4.2 Tonne-Years of Exposure of the LUX-ZEPLIN (LZ) Experiment". arXiv. **hep-ex**: <u>2410.17036</u>. Report number: FERMILAB-PUB-24-0796-V.*

51. <u>^</u>*Nagata N, Shirai S (2015). "Higgsino Dark Matter in High-Scale Supersymmetry". Journal of High Energy Physics. **01** (1): 029. doi:<u>10.1007/JHEP01(2015)029</u>. arXiv:<u>1410.4549</u>.*

52. <u>^</u>*Martin SP (2024). "The curtain lowers on directly detectable higgsino dark matter". arXiv **hep-ph**. Available from: <u>arXiv:2412.08958</u>.*

53. <u>a</u>, <u>b</u>*Dessert C, Foster JW, Park Y, Safdi BR, Xu WL (2023). "Higgsino dark matter confronts 14 years of Fermi γ-ray data". Physical Review Letters. **130** (20): 201001.*

54. <u>^</u>*Rodd NL, Safdi BR, Xu WL (2024). "CTA and SWGO can discover Higgsino dark matter annihilation". Phys. Rev. D. **110** (4): 043003. doi:<u>10.1103/PhysRevD.110.043003</u>. arXiv:<u>2405.13104</u>.*

55. <u>^</u>*Beneke M, Bharucha A, Hryczuk A, Recksiegel S, Ruiz-Femenia P (2017). "The Last Refuge of Mixed Wino-Higgsino Dark Matter". Journal of High Energy Physics. **01** (1): 002. doi:<u>10.1007/JHEP01(2017)002</u>. arXiv:<u>1611.00804</u>.*

56. ^Chen N, Feldman D, Liu Z, Nath P, Peim G (2011). "Higgsino Dark Matter Model Consistent with Galactic Co smic Ray Data and Possibility of Discovery at LHC-7". Physical Review D. **83** (2): 023506. doi:10.1103/PhysRe vD.83.023506. arXiv:1010.0939.

57. ^Beneke M, Hasner C, Urban K, Vollmann M (2020). "Precise yield of high-energy photons from Higgsino da rk matter annihilation". Journal of High Energy Physics. **03** (3): 030. doi:10.1007/JHEP03(2020)030. arXiv:191 2.02034.

58. ^Enberg R, Munir S, Pérez de los Heros C, Werder D (2015). "Prospects for higgsino-singlino dark matter det ection at IceCube and PINGU". arXiv. 1506.05714.

59. ^Bobrovskyi S, Hajer J, Rydbeck S (2013). "Long-Lived Higgsinos as Probes of Gravitino Dark Matter at the L HC". Journal of High Energy Physics. **02** (2): 133. doi:10.1007/JHEP02(2013)133. arXiv:1211.5584.

60. ^Chakraborti M, Chattopadhyay U, Poddar S (2017). "How Light a Higgsino or a Wino Dark Matter Can Bec ome in a Compressed Scenario of {{MSSM}}". Journal of High Energy Physics. **09** (9): 064. doi:10.1007/JHEP 09(2017)064. arXiv:1702.03954.

61. ^Saito M, Sawada R, Terashi K, Asai S (2019). "Discovery reach for wino and higgsino dark matter with a di sappearing track signature at a 100 TeV pp collider". Eur. Phys. J. C. **79** (6): 469. doi:10.1140/epjc/s10052-019- 6974-2. arXiv:1901.02987 [hep-ph].

62. ^Capdevilla R, Meloni F, Simoniello R, Zurita J (2021). "Hunting wino and higgsino dark matter at the muon collider with disappearing tracks". JHEP. **06**: 133. doi:10.1007/JHEP06(2021)133. arXiv:2102.11292.

63. ^Fukuda H, Nagata N, Otono H, Shirai S (2018). "Higgsino Dark Matter or Not: Role of Disappearing Track S earches at the LHC and Future Colliders". Phys. Lett. B. **781**: 306–311. doi:10.1016/j.physletb.2018.03.088. arXi v:1703.09675.

64. ^Giudice GF, Masiero A (1988). "A Natural Solution to the mu Problem in Supergravity Theories". Phys. Lett. B. **206**: 480–484. doi:10.1016/0370-2693(88)91613-9.

65. ^Arvanitaki A, Baryakhtar M, Huang X, van Tilburg K, Villadoro G (2014). "The Last Vestiges of Naturalnes s". JHEP. **03**: 022. doi:10.1007/JHEP03(2014)022. arXiv:1309.3568.

66. ^Evans JA, Kats Y, Shih D, Strassler MJ (2014). "Toward Full LHC Coverage of Natural Supersymmetry". JHE P. **07**: 101. doi:10.1007/JHEP07(2014)101. arXiv:1310.5758.

67. ^Baer H, Barger V, Mickelson D, Padeffke-Kirkland M (2014). "SUSY models under siege: LHC constraints an d electroweak fine-tuning". Phys. Rev. D. **89** (11): 115019. doi:10.1103/PhysRevD.89.115019. arXiv:1404.2277.

68. ^Cao J, Meng L, Yue Y, Zhou H, Zhu P (2020). "Suppressing the scattering of WIMP dark matter and nucleons in supersymmetric theories". Phys. Rev. D. **101** (7): 075003. doi:10.1103/PhysRevD.101.075003.

69. ^Miller DJ, Nevzorov R, Zerwas PM (2004). "The Higgs sector of the next-to-minimal supersymmetric stand ard model". Nucl. Phys. B. **681**: 3–30. doi:10.1016/j.nuclphysb.2003.12.021. arXiv:hep-ph/0304049.

70. a, b, c, d, e, f, gEllwanger U, Hugonie C, Teixeira AM (2010). "The Next-to-Minimal Supersymmetric Standard Model". Phys. Rept.. **496**: 1-77. doi:10.1016/j.physrep.2010.07.001. arXiv:0910.1785.

71. ^Maniatis M (2010). "The Next-to-Minimal Supersymmetric extension of the Standard Model reviewed". In t. J. Mod. Phys. A. **25**: 3505–3602. doi:10.1142/S0217751X10049827. arXiv:0906.0777.

72. ^Hollik WG, Liebler S, Moortgat-Pick G, Paßehr S, Weiglein G (2019). "Phenomenology of the inflation-inspir ed NMSSM at the electroweak scale". Eur. Phys. J. C. **79** (1): 75. doi:10.1140/epjc/s10052-019-6561-6. arXiv:180 9.07371.

73. ^Hollik WG, Weiglein G, Wittbrodt J (2019). "Impact of Vacuum Stability Constraints on the Phenomenology of Supersymmetric Models". JHEP. **03**: 109. doi:10.1007/JHEP03(2019)109. arXiv:1812.04644.

74. ^Cao J, He Y, Shang L, Su W, Zhang Y (2016). "Natural NMSSM after LHC Run I and the Higgsino dominated dark matter scenario". JHEP. **08**: 037. doi:10.1007/JHEP08(2016)037. arXiv:1606.04416.

75. ^Cao J, Jia X, Meng L, Yue Y, Zhang D (2023). "Status of the singlino-dominated dark matter in general Next -to-Minimal Supersymmetric Standard Model". JHEP. **03**: 198. doi:10.1007/JHEP03(2023)198. arXiv:2210.087 69.

76. a, bCao J, Jia X, Lian J (2024). "Unified interpretation of the muon g-2 anomaly, the 95 GeV diphoton, and bb̄ excesses in the general next-to-minimal supersymmetric standard model". Phys. Rev. D. **110** (11): 115039. doi: 10.1103/PhysRevD.110.115039. arXiv:2402.15847.

77. a, b, c, d, e, f, g, hMeng L, Cao J, Li F, Yang S (2024). "Dark Matter physics in general NMSSM". JHEP. **08**: 212. do i:10.1007/JHEP08(2024)212. arXiv:2405.07036 [hep-ph].

78. ^Ellwanger U (1983). "NONRENORMALIZABLE INTERACTIONS FROM SUPERGRAVITY, QUANTUM CORRE CTIONS AND EFFECTIVE LOW-ENERGY THEORIES". Phys. Lett. B. **133**: 187–191. doi:10.1016/0370-2693(83)9 0557-9.

79. a, bAbel SA (1996). "Destabilizing divergences in the NMSSM". Nucl. Phys. B. **480**: 55–72. doi:10.1016/S0550-3 213(96)00470-1. arXiv:hep-ph/9609323.

80. ^Kolda CF, Pokorski S, Polonsky N (1998). "Stabilized singlets in supergravity as a source of the mu – param eter". Phys. Rev. Lett.. **80**: 5263–5266. doi:10.1103/PhysRevLett.80.5263. arXiv:hep-ph/9803310.

81. ^Panagiotakopoulos C, Tamvakis K (1999). "Stabilized NMSSM without domain walls". Phys. Lett. B. **446**: 2 24–227. doi:10.1016/S0370-2693(98)01493-2. arXiv:hep-ph/9809475.

82. [a, b]*Ross GG, Schmidt-Hoberg K (2012). "The Fine-Tuning of the Generalised NMSSM". Nucl. Phys. B. 862: 710 −719. doi:[10.1016/j.nuclphysb.2012.05.007](). arXiv:[1108.1284]().*

83. [∧]*Lee HM, Raby S, Ratz M, Ross GG, Schieren R, Schmidt-Hoberg K, Vaudrevange PKS (2011). "A unique Z_4^R symmetry for the MSSM". Phys. Lett. B. 694: 491−495. doi:[10.1016/j.physletb.2010.10.038](). arXiv:[1009.0905]().*

84. [∧]*Lee HM, Raby S, Ratz M, Ross GG, Schieren R, Schmidt-Hoberg K, Vaudrevange PKS (2011). "Discrete R symmetries for the MSSM and its singlet extensions". Nucl. Phys. B. 850: 1−30. doi:[10.1016/j.nuclphysb.2011.04.009](). arXiv:[1102.3595]().*

85. [∧]*Ross GG, Schmidt-Hoberg K, Staub F (2012). "The Generalised NMSSM at One Loop: Fine Tuning and Phenomenology". JHEP. 08: 074. doi:[10.1007/JHEP08(2012)074](). arXiv:[1205.1509]().*

86. [a, b]*Aad G, et al. (2022). "A detailed map of Higgs boson interactions by the ATLAS experiment ten years after the discovery". Nature. 607 (7917): 52−59. doi:[10.1038/s41586-022-04893-w](). arXiv:[2207.00092](). [Erratum: Nature 612, E24 (2022)].*

87. [a, b]*CMS collaboration, Tumasyan A, et al. A portrait of the Higgs boson by the CMS experiment ten years after the discovery. Nature. 607 (7917): 60−68. doi:[10.1038/s41586-022-04892-x](). arXiv:[2207.00043](). [Erratum: Nature 623, (2023)].*

88. [∧]*Aad G, et al. (2020). "Search for heavy Higgs bosons decaying into two tau leptons with the ATLAS detector using pp collisions at √s=13 TeV". Phys. Rev. Lett.. 125 (5): 051801. doi:[10.1103/PhysRevLett.125.051801](). arXiv:[2002.12223]().*

89. [a, b, c]*Baum S, Carena M, Shah NR, Wagner CE (2018). "Higgs portals for thermal Dark Matter. EFT perspectives and the NMSSM". JHEP. 04: 069. doi:[10.1007/JHEP04(2018)069](). arXiv:[1712.09873]().*

90. [∧]*Lian J (2024). "95 GeV excesses in the Z3-symmetric next-to-minimal supersymmetric standard model". Phys. Rev. D. 110 (11): 115018. doi:[10.1103/PhysRevD.110.115018](). arXiv:[2406.10969]().*

91. [∧]*Pierce A, Shah NR, Freese K (2013). "Neutralino Dark Matter with Light Staus". arXiv. **hep-ph**: [1309.7351]().*

92. [a, b]*Griest K, Seckel D (1991). "Three exceptions in the calculation of relic abundances". Phys. Rev. D. 43: 3191− 3203. doi:[10.1103/PhysRevD.43.3191]().*

93. [∧]*Baker MJ, et al. The Coannihilation Codex. JHEP. 12 (2015): 120. doi:[10.1007/JHEP12(2015)120](). arXiv:[1510.03434]().*

94. [∧]*Drees M, Nojiri MM (1993). "The Neutralino relic density in minimal N=1 supergravity". Phys. Rev. D. 47: 376−408. doi:[10.1103/PhysRevD.47.376](). arXiv:[hep-ph/9207234]().*

95. [a, b]*Drees M, Nojiri MM (1993). "New contributions to coherent neutralino - nucleus scattering". Phys. Rev. D. 47: 4226−4232. doi:[10.1103/PhysRevD.47.4226](). arXiv:[hep-ph/9210272]().*

96. a, b Drees M, Nojiri M (1993). "Neutralino - nucleon scattering revisited". *Phys. Rev. D.* **48**: 3483–3501. doi:10.1103/PhysRevD.48.3483. arXiv:hep-ph/9307208.

97. ^Belanger G, Boudjema F, Pukhov A, Semenov A (2009). "Dark matter direct detection rate in a generic model with micrOMEGAs 2.2". *Comput. Phys. Commun.*. **180**: 747–767. doi:10.1016/j.cpc.2008.11.019. arXiv:0803.2360.

98. ^Alarcon JM, Martin Camalich J, Oller JA (2012). "The chiral representation of the πN scattering amplitude and the pion-nucleon sigma term". *Phys. Rev. D.* **85**: 051503. doi:10.1103/PhysRevD.85.051503. arXiv:1110.3797.

99. ^Alarcon JM, Geng LS, Martin Camalich J, Oller JA (2014). "The strangeness content of the nucleon from effective field theory and phenomenology". *Phys. Lett. B.* **730**: 342–346. doi:10.1016/j.physletb.2014.01.065. arXiv:1209.2870.

100. ^Cao J, Li D, Lian J, Yue Y, Zhou H (2021). "Singlino-dominated dark matter in general NMSSM". arXiv:2102.05317 [hep-ph].

101. ^Zhou H, Cao J, Lian J, Zhang D (2021). "Singlino-dominated dark matter in Z_3-NMSSM". arXiv:2102.05309 [hep-ph].

102. ^Chalons G, Dolan MJ, McCabe C (2013). "Neutralino dark matter and the Fermi gamma-ray lines". *JCAP.* **02**: 016. doi:10.1088/1475-7516/2013/02/016. arXiv:1211.5154.

103. ^Staub F (2008). "SARAH". arXiv:0806.0538 [hep-ph].

104. ^Staub F (2013). "SARAH 3.2: Dirac Gauginos, UFO output, and more". *Comput. Phys. Commun.*. **184**: 1792–1809. doi:10.1016/j.cpc.2013.02.019. arXiv:1207.0906.

105. ^Staub F (2014). "SARAH 4 : A tool for (not only SUSY) model builders". *Comput. Phys. Commun.*. **185**: 1773–1790. doi:10.1016/j.cpc.2014.02.018. arXiv:1309.7223.

106. ^Staub F (2015). "Exploring new models in all detail with SARAH". *Adv. High Energy Phys.*. **2015**: 840780. doi:10.1155/2015/840780. arXiv:1503.04200.

107. ^Porod W, Staub F (2012). "SPheno 3.1: extensions including flavour, CP-phases and models beyond the MSSM". *Computer Physics Communications.* **183** (11): 2458–2469. doi:10.1016/j.cpc.2012.05.021.

108. ^Porod W (2003). "SPheno, a program for calculating supersymmetric spectra, SUSY particle decays and SUSY particle production at e+ e- colliders". *Comput. Phys. Commun.*. **153**: 275–315. doi:10.1016/S0010-4655(03)00222-4. arXiv:hep-ph/0301101.

109. ^Belanger G, Boudjema F, Pukhov A (2013). "micrOMEGAs: a code for the calculation of Dark Matter properties in generic models of particle interaction". In: The Dark Secrets of the Terascale: Proceedings, TASI 2011, Boulder, Colorado, USA, Jun 6 - Jul 11, 2011. pp. 739-790. doi:10.1142/9789814390163 0012. arXiv:1402.0787.

110. ^Porod W, Staub F, Vicente A (2014). "A Flavor Kit for BSM models". Eur. Phys. J. C. **74** (8): 2992. doi:10.1140/epjc/s10052-014-2992-2. arXiv:1405.1434.

111. ^Belanger G, Boudjema F, Pukhov A, Semenov A (2002). "MicrOMEGAs: A Program for calculating the relic density in the MSSM". Comput. Phys. Commun.. **149**: 103–120. doi:10.1016/S0010-4655(02)00596-9. arXiv:hep-ph/0112278.

112. ^Belanger G, Boudjema F, Hugonie C, Pukhov A, Semenov A (2005). "Relic density of dark matter in the NMSSM". JCAP. **09**: 001. doi:10.1088/1475-7516/2005/09/001. arXiv:hep-ph/0505142.

113. ^Belanger G, Boudjema F, Pukhov A, Semenov A (2007). "MicrOMEGAs 2.0: A Program to calculate the relic density of dark matter in a generic model". Comput. Phys. Commun.. **176**: 367–382. doi:10.1016/j.cpc.2006.11.008. arXiv:hep-ph/0607059.

114. ^Belanger G, Boudjema F, Pukhov A, Semenov A (2010). microOMEGAs: a tool for dark matter studies. Available from: arXiv:1005.4133 [hep-ph].

115. ^Belanger G, Boudjema F, Pukhov A, Semenov A (2010). "microOMEGAs: A Tool for dark matter studies". Nuovo Cim. C. **033N2**: 111–116. doi:10.1393/ncc/i2010-10591-3. arXiv:1005.4133 [hep-ph].

116. ^Belanger G, Boudjema F, Pukhov A, Semenov A (2014). "microOMEGAs_3: A program for calculating dark matter observables". Comput. Phys. Commun.. **185**: 960–985. doi:10.1016/j.cpc.2013.10.016. arXiv:1305.0237.

117. ^Barducci D, Belanger G, Bernon J, Boudjema F, Da Silva J, Kraml S, Laa U, Pukhov A (2018). "Collider limits on new physics within microOMEGAs_4.3". Comput. Phys. Commun.. **222**: 327–338. doi:10.1016/j.cpc.2017.08.028. arXiv:1606.03834.

118. ^Be9langer G, Boudjema F, Goudelis A, Pukhov A, Zaldivar B (2018). "microOMEGAs5.0 : Freeze-in". Comput. Phys. Commun.. **231**: 173-186. doi:10.1016/j.cpc.2018.04.027. arXiv:1801.03509.

119. ^Feroz F, Hobson MP, Bridges M (2009). "MultiNest: an efficient and robust Bayesian inference tool for cosmology and particle physics". Mon. Not. Roy. Astron. Soc.. **398**: 1601–1614. doi:10.1111/j.1365-2966.2009.14548.x. arXiv:0809.3437.

120. ^Shang L, Zhang Y (2024). "EasyScan_HEP: A tool for connecting programs to scan the parameter space of physics models". Comput. Phys. Commun.. **296**: 109027. doi:10.1016/j.cpc.2023.109027. arXiv:2304.03636.

121. a, b Fowlie A, Bardsley MH (2016). "Superplot: a graphical interface for plotting and analysing MultiNest output". Eur. Phys. J. Plus. **131** (11): 391. doi:10.1140/epjp/i2016-16391-0. arXiv:1603.00555.

122. ^Matsumoto S, Mukhopadhyay S, Tsai YL (2016). "Effective Theory of WIMP Dark Matter supplemented by Simplified Models: Singlet-like Majorana fermion case". Phys. Rev. D. **94** (6): 065034. doi:10.1103/PhysRevD.94.065034. arXiv:1604.02230.

123. ^Cao J, He Y, Pan Y, Yue Y, Zhou H, Zhu P (2020). "Impact of leptonic unitarity and dark matter direct detecti on experiments on the NMSSM with inverse seesaw mechanism". JHEP. **12**: 023. doi:10.1007/JHEP12(2020)0 23. arXiv:1903.01124.

124. ^XENON collaboration, Aprile E, et al. (2018). "Dark Matter Search Results from a One Ton-Year Exposure of XENON1T". Phys. Rev. Lett.. **121** (11): 111302. doi:10.1103/PhysRevLett.121.111302. arXiv:1805.12562.

125. ^Bechtle P, Heinemeyer S, Stål O, Stefaniak T, Weiglein G (2014). "$HiggsSignals$: Confronting arbitrary Hig gs sectors with measurements at the Tevatron and the LHC". Eur. Phys. J. C. **74** (2): 2711. doi:10.1140/epjc/s10 052-013-2711-4. arXiv:1305.1933.

126. ^Strål O, Stefaniak T (2013). "Constraining extended Higgs sectors with HiggsSignals". PoS. **EPS-HEP2013**: 3 14. doi:10.22323/1.180.0314. arXiv:1310.4039.

127. ^Bechtle P, Heinemeyer S, Stål O, Stefaniak T, Weiglein G (2014). "Probing the Standard Model with Higgs si gnal rates from the Tevatron, the LHC and a future ILC". JHEP. **11**: 039. doi:10.1007/JHEP11(2014)039. arXiv:14 03.1582.

128. ^Bechtle P, Heinemeyer S, Klingl T, Stefaniak T, Weiglein G, Wittbrodt J (2021). "HiggsSignals-2: Probing new physics with precision Higgs measurements in the LHC 13 TeV era". Eur. Phys. J. C. **81** (2): 145. doi:10.1140/epj c/s10052-021-08942-y. arXiv:2012.09197.

129. ^Bechtle P, Brein O, Heinemeyer S, Weiglein G, Williams KE (2010). "HiggsBounds: Confronting Arbitrary Hi ggs Sectors with Exclusion Bounds from LEP and the Tevatron". Comput. Phys. Commun.. **181**: 138–167. doi:1 0.1016/j.cpc.2009.09.003. arXiv:0811.4169.

130. ^Bechtle P, Brein O, Heinemeyer S, Weiglein G, Williams KE (2011). "HiggsBounds 2.0.0: Confronting Neutral and Charged Higgs Sector Predictions with Exclusion Bounds from LEP and the Tevatron". Comput. Phys. C ommun.. **182**: 2605–2631. doi:10.1016/j.cpc.2011.07.015. arXiv:1102.1898.

131. ^Bechtle P, Brein O, Heinemeyer S, Stal O, Stefaniak T, Weiglein G, Williams K (2012). "Recent Developments in HiggsBounds and a Preview of HiggsSignals". PoS. **CHARGED2012**: 024. doi:10.22323/1.156.0024. arXiv:13 01.2345.

132. ^Bechtle P, Brein O, Heinemeyer S, Stål O, Stefaniak T, Weiglein G, Williams KE (2014). "HiggsBounds-4: Impr oved Tests of Extended Higgs Sectors against Exclusion Bounds from LEP, the Tevatron and the LHC". Eur. P hys. J. C. **74** (3): 2693. doi:10.1140/epjc/s10052-013-2693-2. arXiv:1311.0055.

133. ^Bechtle P, Dercks D, Heinemeyer S, Klingl T, Stefaniak T, Weiglein G, Wittbrodt J (2020). "HiggsBounds-5: Te sting Higgs Sectors in the LHC 13 TeV Era". Eur. Phys. J. C. **80** (12): 1211. doi:10.1140/epjc/s10052-020-08557-9. arXiv:2006.06007.

134. ^Carpenter LM, Colburn R, Goodman J, Linden T (2016). "Indirect Detection Constraints on s and t Channel Simplified Models of Dark Matter". Phys. Rev. D. **94** (5): 055027. doi:10.1103/PhysRevD.94.055027. arXiv:1606.04138.

135. ^Boddy KK, Hill S, Kumar J, Sandick P, Shams Es Haghi B (2021). "MADHAT: Model-Agnostic Dark Halo Analysis Tool". Comput. Phys. Commun.. **261**: 107815. doi:10.1016/j.cpc.2020.107815. arXiv:1910.02890.

136. ^Boddy KK, Carter ZJ, Kumar J, Rufino L, Sandick P, Tapia-Arellano N (2024). "New dark matter analysis of milky way dwarf satellite galaxies with madhatv2". Phys. Rev. D. **109** (10): 103007. doi:10.1103/PhysRevD.109.103007. arXiv:2401.05327.

137. ^Zyla PA, Particle Data Group collaboration (2020). "Review of Particle Physics". PTEP. **2020** (8): 083C01. doi:10.1093/ptep/ptaa104.

138. a, b Bahl H, Biekötter T, Heinemeyer S, Li C, Paasch S, Weiglein G, Wittbrodt J (2023). "HiggsTools: BSM scalar phenomenology with new versions of HiggsBounds and HiggsSignals". Comput. Phys. Commun.. **291**: 108803. doi:10.1016/j.cpc.2023.108803. arXiv:2210.09332.

Declarations

Potential competing interests: No potential competing interests to declare.